
Article:

Adams, C., Alborzi, E. orcid.org/0000-0002-2585-0824, Meijer, A.J.H.M. orcid.org/0000-0003-4803-3488 et al. (2 more authors) (2023) Mechanistic investigation into the formation of insolubles in bulk fuel jet fuel using quantum chemical and experimental techniques. Fuel, 334 (Part 1). 126202. ISSN 0016-2361

https://doi.org/10.1016/j.fuel.2022.126202

Mechanistic Investigation Into The Formation of Insolubles in Bulk Fuel Jet Fuel Using Quantum Chemical and Experimental Techniques

Charlie Adams[a], Ehsan Alborzi[a], Anthony J.H.M. Meijer[b], Kevin J. Hughes[a], Mohamed Pourkashanian[a]

[a] *Department of Mechanical Engineering The University of Sheffield, S3 7HF, UK*
[b] *Department of Chemistry The University of Sheffield, S3 7HF, UK*

Abstract

The SMORS mechanism describing the formation of insoluble material in bulk jet fuel was investigated using density functional and experimental techniques. The first part of the SMORS mechanism, the formation of quinones from the oxidation of indigenous fuel phenols, was shown to proceed via two possible pathways. First, a single-step pathway yielding two quinones and a hydrogen peroxide. Secondly, a two-step pathway yielding a quinone, p-chinole and singlet oxygen. The second step of the SMORS mechanism, the reaction of quinones with electron-rich heterocyles in fuels, was shown to proceed via a homolytic aromatic substitution pathway. These findings, allow us to propose a modified SMORS mechanism, built on our enhanced mechanistic understanding of fuel deposit formation.

1. Introduction

Liquid-phase jet fuel thermal oxidative degradation in conventional fuels is largely driven by minor heteroatomic species.[1] The process of jet fuel thermal degradation can be split into three main stages: 1) autoxidation of the bulk fuel yielding oxidized species, 2) agglomeration of oxidized components to high molecular weight species, 3) formation of insolubles.[2] There is a better understanding of step 1 than step 2, and this is reflected in the existing pseudo-detailed mechanisms for deposition, where there are more steps representing autoxidation reactions.[3, 1, 4]

*Charlie Adams
**Ehsan Alborzi

Preprint submitted to Fuel *6th September 2022*

Email addresses: bismuthadams@sheffield.ac.uk (Charlie Adams), e.alborzi@sheffield.ac.uk (Ehsan Alborzi), a.meijer@sheffield.ac.uk (Anthony J.H.M. Meijer)

To understand the agglomeration and insoluble formation processes in more detail, researchers have taken the approach of correlating initial polar concentrations with mass of deposit.[5, 6, 7] Phenols and electron-rich nitrogen compounds, indoles and carbazoles, were found to correlate well with mass of deposit.[7] In fact, phenol and electron-rich nitrogen compounds have been found to interact synergistically to enhance deposit formation in fuels.[6, 8] To explain this synergistic effect, Beaver *et al.* proposed the Soluble Macromolecular Oxidatively Reactive Species (SMORS) mechanism.[9] The SMORS mechanism was originally based on work by Hardy and Wechter. Hardy and Wechter identified nitrogen and oxygen containing deposit precursors using methanol extraction, where Beaver *et al.* proposed these precursors to form from quinone-aromatic coupling species. Several articles have subsequently used this mechanism to explain observed deposition effects,[10, 11, 12, 13] but none have explored the SMORS mechanism in depth.

The original SMORS mechanism proposed by Beaver *et al.* is described in detail in the following reference[9] and in Figure 1. It relies on the formation of electrophilic quinones from the oxidation of phenol. These quinones are then proposed to undergo electrophilic aromatic substitution reactions (EAS) with electron-rich heteroatomic compounds in fuel.[14] Using indole as a model for nitrogen heterocycle leads to the formation of a 3-indolyl hydroquinone. The EAS product between quinone and nitrogen heterocycles is proposed to undergo further EAS steps to successively larger structures, ultimately forming insoluble particles in fuel.[10]

In recent years, density functional theory (DFT) has become an increasingly popular tool to investigate thermal oxidative reactions in fuel.[16, 17, 18, 19] DFT rests upon the assumption that the electron density in an atom/molecule is related to the ground state energy of the system, which in turn can be used to calculate thermochemical and kinetic parameters of reaction systems.[20] Early work by Zabarnick *et al.* used the B3LYP//6-31G(d) level of theory to investigate X−H bond dissociation energies of various fuel heteroatoms to understand their chain-breaking properties.[17] Building on these methods, Parks et al. used the B3LYP//cc-pVTZ level of theory to propose a copper catalyzed hydroperoxide decomposition cycle.[16] Further work by Parks et al. successively elucidated thermally oxidation pathways of a variety of sulfur classes.[18]

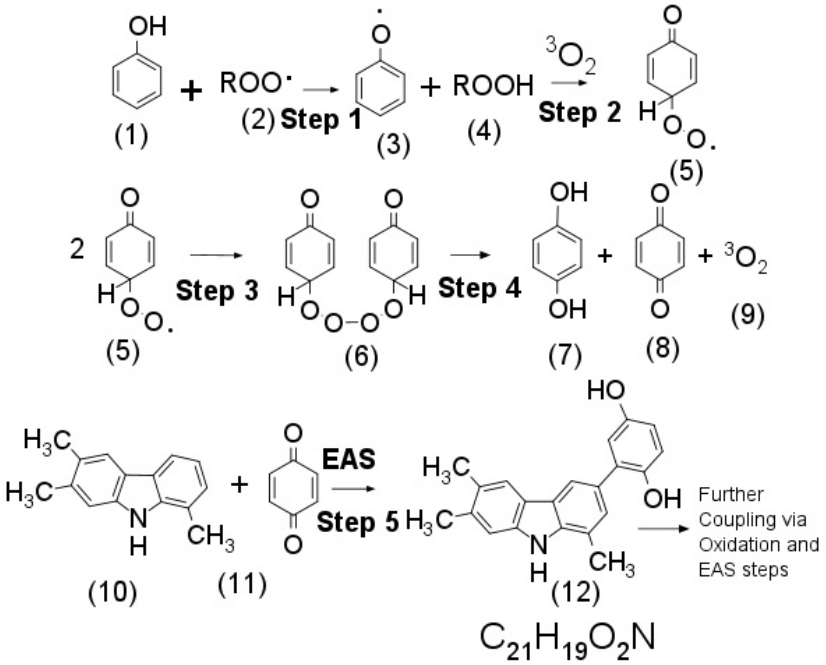

Figure 1: SMORS mechanism as described in reference[9]. The compound **(12)** is found as an extract in Hardy and Wechter's original paper.[15]

It is the aim of this work to investigate the proposed SMORS mechanism at a molecular level using DFT methods, while proposing alternative pathways where appropriate. Additionally, our DFT calculations will enhance the understanding of the SMORS mechanism itself, and allow us to propose alternative pathways. Moreover, a greater mechanistic understanding of the SMORS mechanism will eventually lead to enhanced predictive capabilities in the form of pseudo-detailed mechanisms.

2. Materials and Methods

2.1. Computational Details

All calculations were performed in Gaussian09 (E.01) using the B3LYP functional.[21][22] Grimme's DFT-D3(BJ) dispersion correction was applied to all the calculations to account for long-range effects.[23] A PCM solvation model, with *n*-dodecane as the chosen solvent, was selected to replicate the hydrocarbon bulk.[24] The basis set chosen was cc-pVTZ on an *ultrafine* grid,

this basis set adds polarization functions, thus orbital hybridization can be taken into account.[25] Transition states were optimized using the QST1/3 method depending on the reaction studied. All transition states were verified by the presence of one imaginary frequency corresponding to the saddle point. Additionally, intrinsic reaction coordinate (IRC) calculations were performed to verify the transition state corresponded to the expected reactants and products. Unrestricted (broken symmetry) calculations were performed on open-shell systems, where the HOMO and LUMO were mixed (`guess=mix` option). Entropy values were corrected using the GoodVibes script, which employs a quasi-harmonic correction corrected at 298 K.[26, 27, 28] The quinone oxidation pathway in Section 3.2 was further validated with single point DLPNO-CCSD(T)[29, 30, 31, 32, 33] calculations using the ORCA quantum chemistry package.[34] DLPNO-CCSD(T) allows near CCSD(T) accurate calculations at a fraction of the cost by identifying electron pairs with significant contributions to correlation energy, where the correlation energies for the other pairs are obtained at the MP2 level of theory.

2.2. Surrogate Fuels

The details of the experimental setup can be found in the supporting information (Section 4).

3. Results and Discussion

In this section we will present the DFT calculations for each step of SMORS, in conformity with reference.[9]

3.1. Formation of the Keto-Peroxyl Radical

The first set of calculations was focused on the generation of keto peroxyl radical, indicated as (**P1**) in Figure 2. In the generalized SMORS reaction scheme, the first step involves the abstraction of a hydrogen atom from a phenol (representing an indigenous antioxidant) by a hydroxy radical ROO$\cdot$. As shown in Figure 2, the Gibbs free energy barrier corresponding to the transition state of this reaction (**TS1**) is $\Delta_{\ddagger}G$=+12.65 kcal mol^{-1}; the overall reaction is slightly endergonic, with a $\Delta_r G$(ROO$\cdot$)= +0.40 kcal mol^{-1}.

Comparing the hydrogen abstraction step for the reaction between phenol and different n-dodecane fuel radical classes (R$\cdot$, RO$\cdot$, ROO$\cdot$)[1], the RO$\cdot$ pathway provides the lowest barriers. The calculated values for each pathway

Species	$\Delta_{\ddagger}S$ (kcal mol^{-1}K^{-1})	$\Delta_{\ddagger}H$ (kcal mol^{-1})	$\Delta_{\ddagger}G$ (kcal mol^{-1})	$\Delta_{r}S$ (kcal mol^{-1}K^{-1})	$\Delta_{r}H$ (kcal mol^{-1})	$\Delta_{r}G$ (kcal mol^{-1})
R $\cdot$	-2.749E-02	8.24	9.97	-1.440E-03	-18.88	-17.98
RO $\cdot$	-2.037E-02	0.29	1.32	1.24E-03	-3.31	-20.79
ROO $\cdot$	-2.327E-03	8.94	10.40	9.00E-06	0.40	0.40

Table 1: Calculated energy change of reaction $\Delta_{\ddagger}$ and formation Δ_r values for reaction of phenol with different dodecane fuel radicals calculated at the B3LYP-D3//cc-pVTZ n-dodecane PCM level of theory. Enthalpy values are corrected with GoodVibes at 298K. All $\Delta_{\ddagger}$ values are calculated from stable pre-collision complexes located from an IRC calculation.

associated for each radical class are presented in Table 1 and the comparison for each pathway is shown in Figure 2. The higher associated barriers $\Delta_{\ddagger}G$ for the R $\cdot$ and ROO $\cdot$ species compared to RO $\cdot$ are likely due to the higher level of distortion associated with these barriers. Energies of formation $\Delta_r G$ for the radical classes go from highest to lowest RO $\cdot$ $>$ R $\cdot$ $>$ ROO $\cdot$. The ability of the electron-rich oxygens to share spin density with the ring can justify the lower peroxyl radical reactivity, leading to enhanced radical stability. Whereas the alkyl radical is stabilized solely by the inductive effects from the adjacent carbons.[35]

The next step in the SMORS mechanism is the reaction of dissolved oxygen with the resulting phenoxy radical. In order to study this step computationally, triplet oxygen was selected for the calculation, because of its higher stability and commonality in nature.[36] Our results indicate that the reaction between dissolved oxygen and the phenoxy radical is endothermic, with a $\Delta_r G$=+15.23 kcal/mol. The transition state with a barrier of $\Delta_r G$=+21.50 kcal/mol was identified for this reaction (**TS2** in Figure 2), which is in good agreement with the previous work.[37] Overall, the formation of keto-peroxyl radical (**P1** in Figure 2) is endergonic, indicating that high temperatures would be needed for this species to form. However, the exergonicity of the reactions of phenol with R $\cdot$ and RO $\cdot$ more than compensates for this, making the hydrogen abstraction using R $\cdot$ or RO $\cdot$ exergonic overall

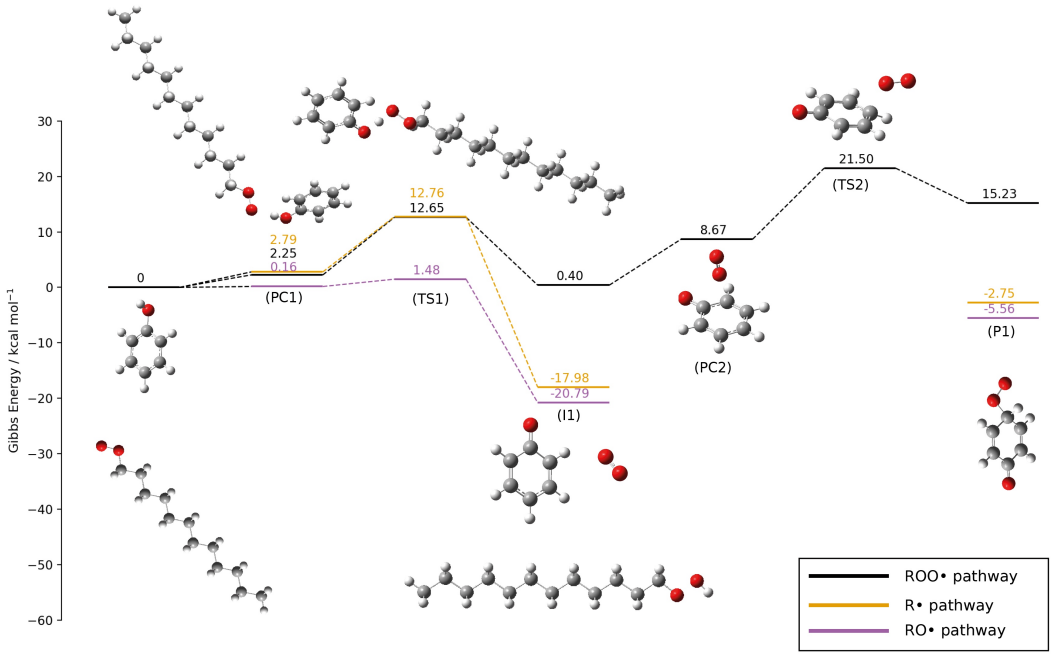

Figure 2: Potential energy surface (Gibbs energy) for the formation of the keto peroxyl radical calculated at the B3LYP-D3//cc-pVTZ level of theory using *n*-dodecane (PCM) as a solvent.

and making these reactions more favorable than the reaction with ROO· Nevertheless, the concentration of these chain-carrying radicals will be important too, with ROO· being primary chain carriers due to their higher concentration.[2]

3.2. Formation of Quinones

The next step proposed in the SMORS mechanism is the chain termination of two keto peroxyl radicals, resulting in the formation of a quinone, a hydroquinone and oxygen. Quinones have been found to form from substituted and unsubstituted phenols in fuels under oxidative conditions.[38, 4] The formation of quinones from phenols is universally found to occur *via* a termination step.[39, 40, 41] In the SMORS mechanism proposed by Beaver *et al.*

it has been suggested that this step is likely to proceed with the formation of a tetraperoxide (ROOOOR) intermediate, formed from the recombination of two keto-peroxyl radicals. Beaver *et al.* then propose quinones are formed by the decomposition of the ROOOOR via a Russell Mechanism decomposition, leading to the final products.[42] However, our DFT calculations suggest that this is unlikely. The final SMORS species are 104.89 kcal mol^{-1} (indicated as the red level in Figure 3) lower than the starting state of keto-peroxyl radicals. However, it is highly unlikely that the α hydrogen (labelled as 1 in Figure 3) would be able to move to the para-oxygen (labelled as 2 in Figure 3), given that the distance of 4.75 Å is prohibitive to hydrogen transfer. Indeed no transition state was found for this hydrogen transfer.

Because the termination of two radicals is unlikely, the production of keto-peroxyl radicals and subsequent tetroxide formation in competition with *n*-dodecane autoxidation and other phenol H-abstraction pathways was explored using a pseudo-detailed mechanism. The details of the pseudo-detailed mechanism are presented in Section 5. The final concentrations of the species from our pseudo-detailed mechanism is presented in Table 5. Despite the competing steps, the formation of the tetroxide is still competitive with the other autoxidation and hydrogen abstraction steps, with the concentrations greater or similar to *n*-dodecane autoxidation products found.

Alternative to the proposed oxidation products in reference [9], several pathways yielding a p-chinole (**a**), quinone (**b**), and singlet oxygen (**c**). These are shown as **P2a,b,d** in Figure 3. Additionally, a pathway yielding two quinones (**a**) and hydrogen peroxide (**d**) were found (**P2c** in Figure 3).

The first step is the formation of the tetraperoxide. A barrier of 13.36 kcal mol^{-1} (**TS3**) for peroxyl radical recombination and the formation of the tetraperoxide (**I2**) was found in our calculations, which is similar to the previous work on peroxyl radicals.[43]. Furthermore, the formation of the tetraperoxide (**I2**) is endergonic, with a Gibbs energy +8.05 kcal mol^{-1} above the separated species. This can be attributed to the instability of the linear ROOOOR structure.[44] It is worth mentioning that no stable ROOOOR species was found on the triplet surface, which is in agreement with previous work.[45]

The decomposition of ROOOOR can proceed through several pathways which are discussed here. First, a modified Russell Mechanism pathway was explored,

leading to the formation of quinone (**I2** → **TS4a** → **P2a,b,d**) However, the Russell mechanism pathway was found to have a high Gibbs free energy barrier of $\Delta_{\ddagger}G$=+34.91 kcal mol^{-1} . Such a high energy barrier indicates that the Russell mechanism is unlikely to contribute significantly to quinone formation, when compared to other calculated pathways in this section. We note that experimental work has found little evidence for the Russell Mechanism[42] in peroxyl self-reactions producing ROH, RCHO and O_2 products.[46, 47, 48]

Given that the Russell Mechanism decomposition of the tetraperoxide was found to have a large free energy barrier, we considered other pathways. As a consequence, an exergonic single-step channel was identified (**I2** → **TS4c** → **P2c**), yielding a two quinones and a hydrogen peroxide **P2c**. First, the tetraperoxide decomposes via **T4c** ($\Delta_{\ddagger}G$=10.87 kcal mol^{-1}), predicting a simultaneous transfer of two α-hydrogens to two oxygens in the ROOOOR chain and the cleavage of two O-O bonds. The IRC calculation for this transition state can be found in Figure 1 in the SI. Production of hydrogen peroxide from peroxyl self-reactions has been detected in previous work.[41] But, to the best of our knowledge, this is the first time a concerted hydrogen peroxide production step has been located.

A second pathway consists of a two-step channel yielding a quinone, p-chinole, and singlet oxygen species was identified (**I2** → **TS4b** → **I3b** → **TS5b** → **P2a,b,d**). This includes a transition state **TS4b** ($\Delta_{\ddagger}G$=25.27 kcal mol^{-1}) involving a simultaneous cleavage of one O-O and transfer of an α-hydrogen to an oxygen. The resultant intermediate formed (**I3b**) is a stable hydrotrioxide (ROOOH) species hydrogen bonded to a quinone species ($\Delta_r G$=−51.58 kcal/mol). Subsequently, the hydrotrioxide species can decompose via a transition state **TS5b** of $\Delta_{\ddagger}G$=44.26 kcal/mol, characterized by a four membered cyclic structure. This level of energy barrier is in agreement with the previous work.[45, 43] The high barriers for **TS4b** and **TS5b** show that this channel is prohibitive for the production of quinone.

Finally, a further two-step channel leading to a quinone, p-Chinole and singlet oxygen species was identified (**I2** → **I3d** → **TS5d** → **P2a,b,d**). The first step in this pathway is the exergonic decomposition of the ROOOOR species ($\Delta_r G$=-3.27 kcal mol^{-1}), yielding two keto hydroxyl radicals and a singlet oxygen.[49, 50] In a related work, a potential energy surface scan of the CCSD//6-31G(d) level of theory on this step with ethane peroxyl

radicals indicates that this is a barrierless process.[43] In our case also, no transition state was found. Following the decomposition of the tetraperoxide, an α-hydrogen from one peroxyl radical is then transferred linearly to the other peroxyl O atom, yielding **P2a,b,d** with an energy barrier of $\Delta_{\ddagger}G$=+18.84 kcal mol^{-1} corresponding to **TS5d** in Figure 3.

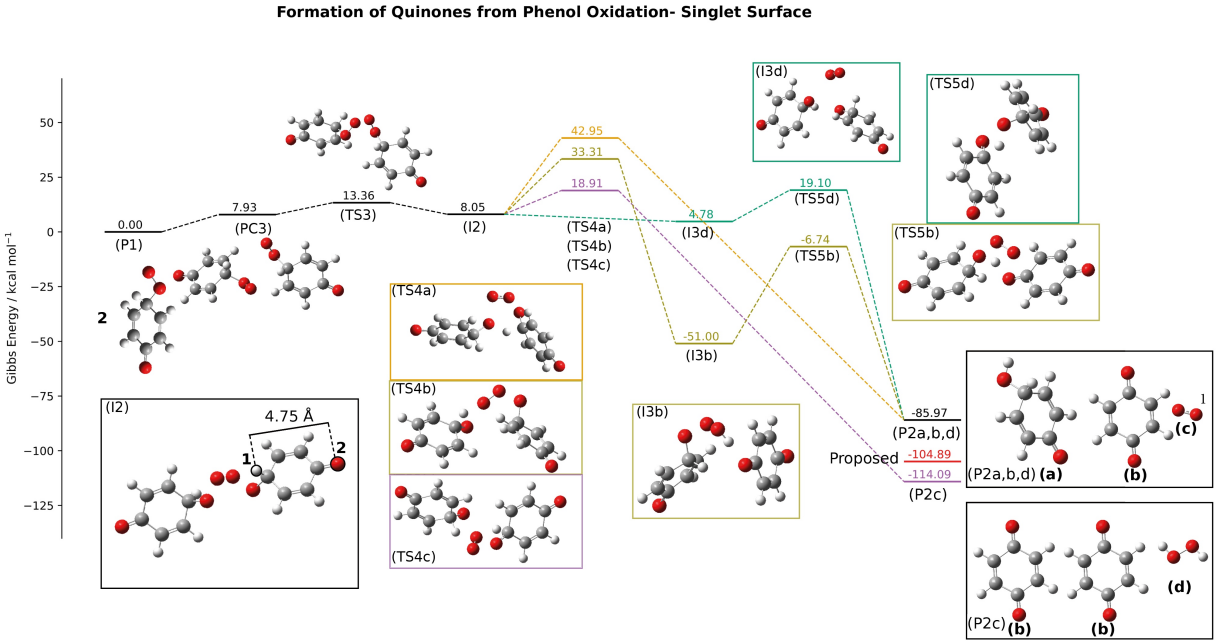

Figure 3: Potential energy surface (Gibbs energy) of the keto-peroxyl radical yielding quinones on the singlet surface, calculated at the B3LYP-D3//cc-pVTZ using n-dodecane (PCM) as a solvent. The red level indicates energy of the proposed quinone oxidation products, where no pathway could be found to form them.

To identify competing oxidation pathways, other non-quinone producing pathways were considered, as shown in Figure 4. On the singlet surface, an exergonic aromatic substitution pathway is identified, leading to ROOR species and singlet oxygen (**P1** $\rightarrow$ **PC4a** $\rightarrow$ **TS6a** $\rightarrow$ **P4**), without producing quinone. In this pathway, at **TS6a** a rocking movement of the peroxyl radical towards an α-carbon on the other peroxyl radical is observed. This is in association

with the simultaneous cleavage of a C−O liberating singlet oxygen is observed. However, the high energy barrier of **TS6a** ($\Delta_{\ddagger}G$=+59.46 kcal mol^{-1}) means that the termination of ROOOOR (**I2**) via **TS3** is strongly preferred, suggesting this pathway can be excluded.

On the triplet surface, an exergonic pathway was identified, which leads to the production of two hydroxy radicals and a triplet oxygen (**P1** → **PC4b** → **TS6b** → **P3**). The first step of this pathway is the formation of a dimeric pre-reaction complex (**PC4b**). Following **PC4b**, a high energy transition state (**TS6b**) was characterized via the simultaneous scission of O−O bonds on each peroxyl radical and the formation of new O−O bonds between terminal oxygens. The very high barrier associated with **TS6b** ($\Delta_{\ddagger}G$=+51.49 kcal/mol) means that this pathway will not proceed beyond **PC4b**.

If all the pathways are compared, then the formation and decomposition of ROOOOR via two routes offers the most likely pathway to quinones with both having similar kinetic barriers. First, the single-step pathway (**I2** → **TS4c** → **P2c**) giving two quinones and hydrogen peroxide. Secondly, the two-step pathway (**I2** → **I4d** → **TS5d** → **P2a,b,d**), yielding a quinone, p-chinole and singlet oxygen. The single-step pathway is more favorable thermodynamically, with an exergonicity of the reaction of 28.12 kcal mol^{-1} lower. Nevertheless, both pathways have similar kinetic barriers. Thus, there is likely to be a distribution of products.

DLPNO-CCSD(T) calculations were performed for the pathways in this section, where the same reactive trend was observed, which validates our method chosen. The results are shown in Section 3 of the supporting information.

In real fuels, unsubstituted phenols form a majority of phenolic species. Nevertheless, they also form quinones when oxidized, and are expected to undergo similar reactions here.[38, 51] Nonetheless, this should be investigated further.

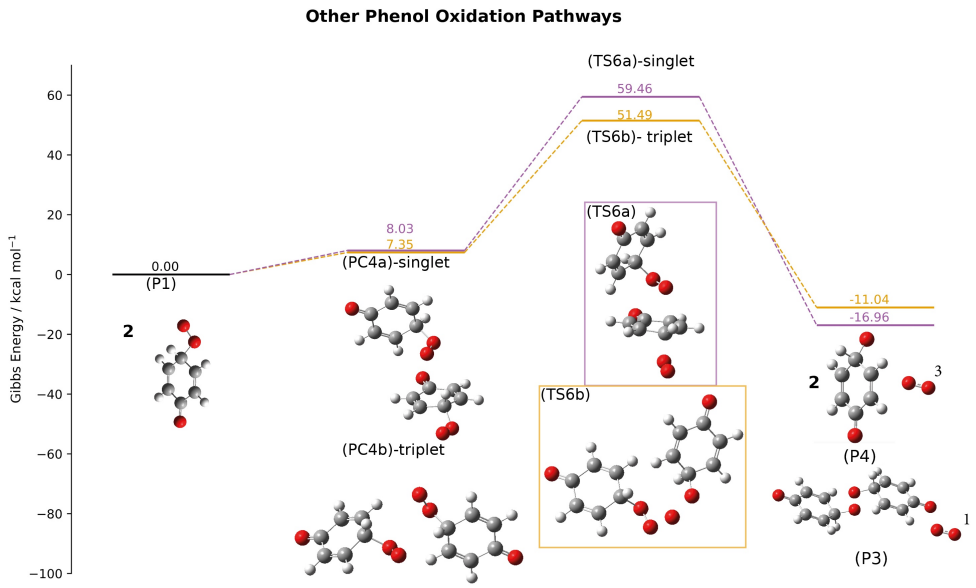

Figure 4: Reactions of Keto-Peroxyl Radical yielding non-quinone products on the triplet and singlet surfaces, calculated at the B3LYP-D3/cc-pVTZ *n*-Dodecane PCM level of theory

3.3. Quinone Heteroatom Coupling Step

3.3.1. Proposed SMORS Electrophilic Aromatic Substitution Step

The next step in the originally proposed SMORS mechanism; the electrophilic aromatic substitution (EAS) between indigenous electron-rich compounds and electrophilic quinones was found to be thermodynamically and kinetically prohibited. EAS reactions usually proceed with the initial attack of an electron-rich aromatic (the carbazole in this case) to an electron deficient species (quinone in our study), breaking aromaticity. The second step is the subsequent release of a species, most commonly H^+, at the site of electrophilic attack, completing the substitution reaction and re-establishing aromaticity.[52] The EAS between indole and benzoquinone (**P2**) proposed

by Beaver *et al.* is presented in Figure 5.[9]. Following the addition of benzoquinone, a zwitterionic σ-complex forms (Indole+Quinone-).[53]

Following the EAS scheme in Figure 5, no stable intermediate was found. The aprotic nature of n-dodecane solvent is unable to provide stability to the charged intermediate. However, even with a PCM water solvent model no stable benzoquinone-indole intermediate structure was found.

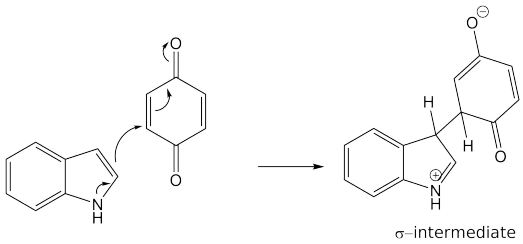

Figure 5: Proposed SMORS EAS step

Despite these limitations, the EAS transition state was identified between methyl substituted-carbazole proposed in Beaver *et al.*[9] and quinone, using a lower level of theory (B3LYP//cc-pvDZ). The intermediate product (**I4**) could only be obtained from a constrained optimization by freezing the C−C bonds. Without freezing the C−C bonds, the zwitterionic structure in 5 optimized to two separate indole and quinone species. The $\Delta_{\ddagger}G$=+177.11 kcal mol^{-1} barrier between benzoquinone and carbazole implies the original SMORS EAS proposal is kinetically prohibited. Recent work on EAS reactions indicate that in aprotic/apolar solvents interactions are likely to proceed through a concerted route, precluding the formation of a charged intermediate. The concerted routes studied found that in apolar solvents tend to involve autocatalysis of the attacking electrophile with another electrophile.[54, 55] Two quinone species reacting with a single indole was studied to explore an autocatalytic concerted route. However, in our case no concerted route to the coupled SMORS species was identified.

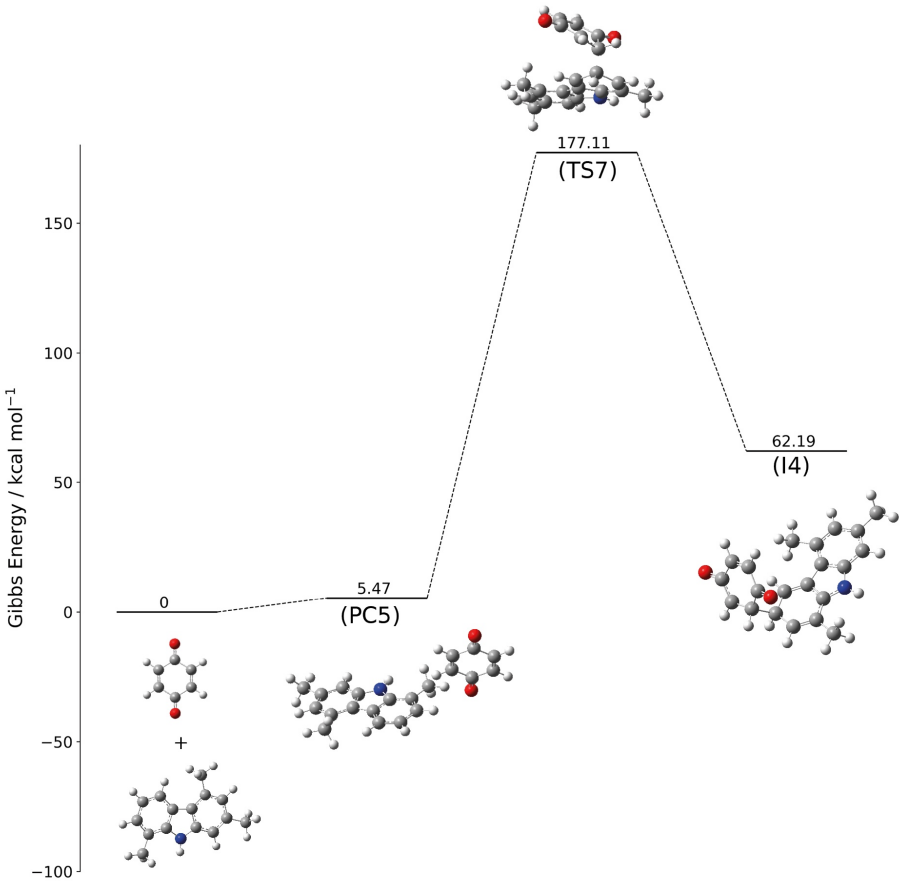

Figure 6: Potential energy surface (Gibbs free energy) of the reaction between carbazole and quinone, calculated at the B3LYP//cc-pVDZ *n*-Dodecane PCM level of theory.

3.3.2. Alternative Acid-Catalyzed EAS Step

The condensation reaction between benzoquinones and indoles has been reported previously to be catalyzed by acid.[56, 57] In fuels, it is proposed that the autoxidation of indigenous sulfur compounds can lead to the formation of sulfonic acids.[18] In addition, previous work has suggested that strong acids may play a role in catalyzing deposit formation.[2] Therefore, an acid-catalyzed pathway was considered as a possible route for SMORS formation.

This alternative SMORS scheme is presented in Figure 7. A protonated quinone was selected to model this pathway since protonation of the indole would preclude it from reacting with the electrophilic quinone species. From the overall reaction scheme presented in Figure 7, it can be concluded that a protonated quinone is able to proceed through a more favorable kinetic pathway. In addition, the formation of the aromatized hydroquinone carbazole species as proposed in the SMORS mechanism is possible and thermodynamically favorable ($-78.13\,\mathrm{kcal\,mol^{-1}}$).

The pre-reaction complex (**PC5**) for this reaction is exergonic. The barrier of the addition step (**TS7**) is small at $\Delta_{\ddagger}G$=+6.83 kcal mol^{-1} above **I5**. When compared to the non-catalyzed EAS scheme (Figure 5), the positive charge delocalized around the quinone species will activate the nucleophilic 3-position of the quinone. A hydrogen transfer (**TS8**) is then achieved through a pseudo-ring like structure, with a small barrier of $+7.10\,\mathrm{kcal\,mol^{-1}}$. The resultant structure from this hydrogen transfer contains a hydroquinone moiety (**I6**). The formation of this species is thermodynamically favorable with an Gibbs free energy change of -18.43 kcal mol^{-1} compared to the starting structures.

Protonation of quinone will also proceed with a barrier. In our DFT calculations the quinone was protonated by a dodecane sulfonic acid, known to form from the oxidation of indigenous sulfur compounds in fuel. It was found that the protonation step was barrierless but highly endergonic in n-dodecane with a large thermodynamic barrier of $\Delta_r G$=+77.57 kcal mol^{-1}. As shown in Figure 7, an overall Gibbs energy of -0.59 kcal mol^{-1} change is associated with the entire catalytic cycle, from the protonation of the quinone by the dodecane sulfonic acid to the formation of the SMORS species. This

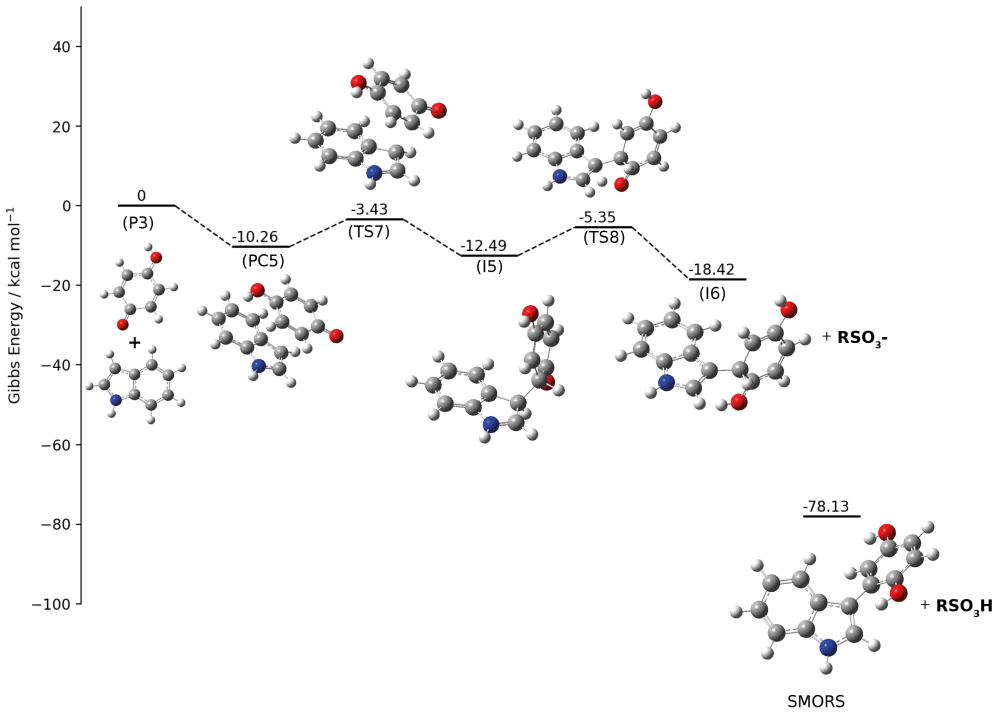

Figure 7: Acid catalyzed EAS step calculated at the B3LYP//cc-pVTZ n-Dodecane PCM level of theory.

indicates that the overall pathway is only mildly exergonic. Nevertheless, a protonated quinone allows the EAS step to proceed with modest kinetic barriers. However, with such a large thermodynamic barrier to quinone protonation in n-dodecane, protonation is unlikely unless the resultant ionic species are stabilized by a more polar solvent. The protonation step in water was calculated to have a thermodynamic cost of $\Delta_r G$=+25.43 kcal mol^{-1}. Small amounts of water have been detected as micelles in jet fuel.[58] We hypothesize that these micelles could offer a site for protonation in fuels.

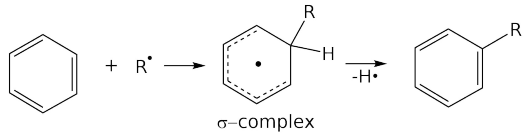

Figure 8: Generalized HAS mechanism.[61]

3.3.3. Alternative Oxidative Coupling Pathway

Although an acid catalyzed pathway was shown to proceed with modest kinetic barries, protonation of quinone in n-dodecane comes at a high thermodynamic cost. Therefore, we investigated additional mechanisms. Another possible pathway for the coupling between indoles and quinones in the SMORS mechanism is an oxidative coupling route. Oxidative coupling products have previously been detected in real and surrogate fuels.[38, 12] Undeniably, chain termination between an indole and a quinone radical would occur spontaneously. However, the termination of two dissimilar radical species is unlikely due to the low concentration of free-radicals in solution.[41, 59] Nevertheless, the termination reaction between an indole and a quinone radical will lead to a small proportion of SMORS. Alternatively, we investigated the possibility of a homolytic aromatic substitution (HAS) reaction between indole radicals and quinone, and indoles and quinone radicals. HAS has been described as the 'radical analogue of the more facile EAS'.[60] In our study an EAS pathway could not be located. Therefore HAS serves as another alternative pathway to forming the SMORS product.

The general HAS mechanism is presented in Figure 8. The first step is manifested by the attack of a radical species on an aromatic ring. The formation of a σ-complex (analogues to the Wheland intermediate in Figure 5) is then followed by the loss of hydrogen leading re-aromatization of the ring.

Following the HAS framework, the scheme depicted in Figure 8 is proposed for the reaction of quinone radical with an indole. The σ-complex formed from the initial attack of the quinone radical at the indole **C3** site is presented as **I8b**. It appears that the formation of the hydroquinone moiety is not immediately accessible *via* abstraction of a hydrogen atom from the σ-complex, which is how the general HAS mechanism proceeds (Figure 8). Instead, internal hydrogen transfer leads to the formation of intermediate **I9**, which contains a

semiquinone moiety. Semiquinones are known for their exceptional stability owing to their resonance stabilization.[37] Nevertheless, hydrogen abstraction from indigenous fuel compounds (RH in Figure 8) will lead to the formation of the SMORS product.

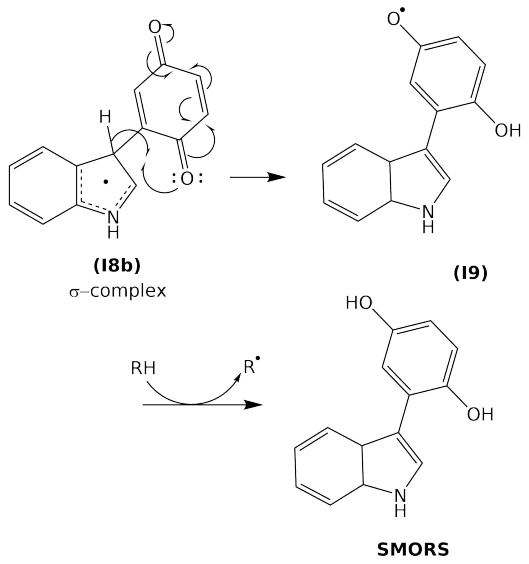

Figure 9: HAS mechanism applied to the SMORS indole + quinone substitution step

DFT calculations for the HAS pathway are presented in Figure 10. For comparison, two HAS reaction pathways were calculated for quinone and indole radicals respectively. For indole, multiple positions for hydrogen abstraction are available, but the **C3** is generally the preferred site for C-C bond formation.[62] Our calculations indicate that the route leading to the formation of quinone radicals is kinetically and thermodynamically preferred (**0→PC6b→TS9b→I7b**) over the formation indole radicals (**0→PC6a→TS9a→I7a**). The transition state for both species is characterized by a linear hydrogen transfer to a dodecane hydroxy radical, where the barrier to quinone hydrogen abstraction (**TS9b**) is 5.04 kcal mol^{-1} lower in Gibbs free energy than the indole abstraction barrier (**TS9a**). Additionally, the resultant quinone radical (**I7b**) is 8.12 kcal mol^{-1} lower in energy than the indole radical (**I7a**). Here it must be noted that when comparing all the products formed from the quinone production (**P2**), hydrogen abstraction

from p-chinole (**(a)P2**) is strongly preferred over quinone due to the formation of a highly stable semiquinone radical. Not shown in Figure 10, the abstraction of an α-hydrogen from p-chinole (**(a)P2**) has a $\Delta_{\ddagger}G$+5.54 kcal mol^{-1} barrier and a resultant $\Delta_r G$ −47.13 kcal mol^{-1}. Consequently, the p-chinole species is more likely to form radicals than indole and quinone here. However, the subsequent attack of the p-Chinole radical at the **C3** of an indole to form a HAS σ-complex has a high barrier $\Delta_{\ddagger}G$ 36.47 kcal mol^{-1}, meaning it can be precluded as a contributor to the HAS pathway.

The next step in the HAS scheme is the attack of the radical to the aromatic ring forming a σ-complex. With respect to the indole radical + quinone pathway, 1,4-benzoquinones are not strictly aromatic. Nevertheless, it has been noted that both substituted and non-substituted 1,4-benzoquinones are able to form resonance structures which could stabilize the resultant σ-intermediate.[63] Both the quinone and indole radical attack pathways (**I7**→**PC7**→**TS10**→**I8**) proceed exergonically. However, in relation to **I7**, the attack of a quinone radical has a lower free-energy barrier (**TS10b**) $\Delta_{\ddagger}G$=6.87 kcal mol^{-1} compared to the attack of the indole radical (**TS10a**) $\Delta_{\ddagger}G$=8.09 kcal mol^{-1}. For both **TS10a** and **TS10b**, the transition state is characterized by a rocking motion between the C−C bonds formed. The resultant indole radical-quinone σ-intermediate (**I8a**) is 4.84 kcal mol^{-1} more stable than the quinone radical-indole σ-intermediate (**I8b**).

Following the formation of the σ-intermediates, a subsequent hydrogen transfer leads both intermediates to form **I9** which is a stable semiquinone radical. Formation of **I9** is strongly preferred from quinone radical-indole σ-intermediate (**I8b**→**TS11b**→**I9**). The free energy barrier for **TS11b** is small ($\Delta_{\ddagger}G$=2.76 kcal mol^{-1}). The re-aromatization step **TS11b** for this pathway is characterized by a pseudo-cyclic transition state structure, where a hydrogen from the **C3** position on the indole is transferred to a quinone (=O) moiety ortho- to the C−C bond. By contrast, re-aromatization of the indole radical-quinone intermediate **I8b** proceeds via a high energy barrier (**TS11a**) $\Delta_{\ddagger}G$=47.64 kcal mol^{-1} meaning this pathway should be discounted as a major HAS pathway. **TS11a** is part of a hydrogen transfer from the quinone **C2** carbon, where the planar quinone moiety has to be bent to allow hydrogen transfer. This bending of the quinone moiety out-of-plane likely leads to the high barrier for **TS11a**.

The final step to produce the resultant **SMORS** species leading to re-

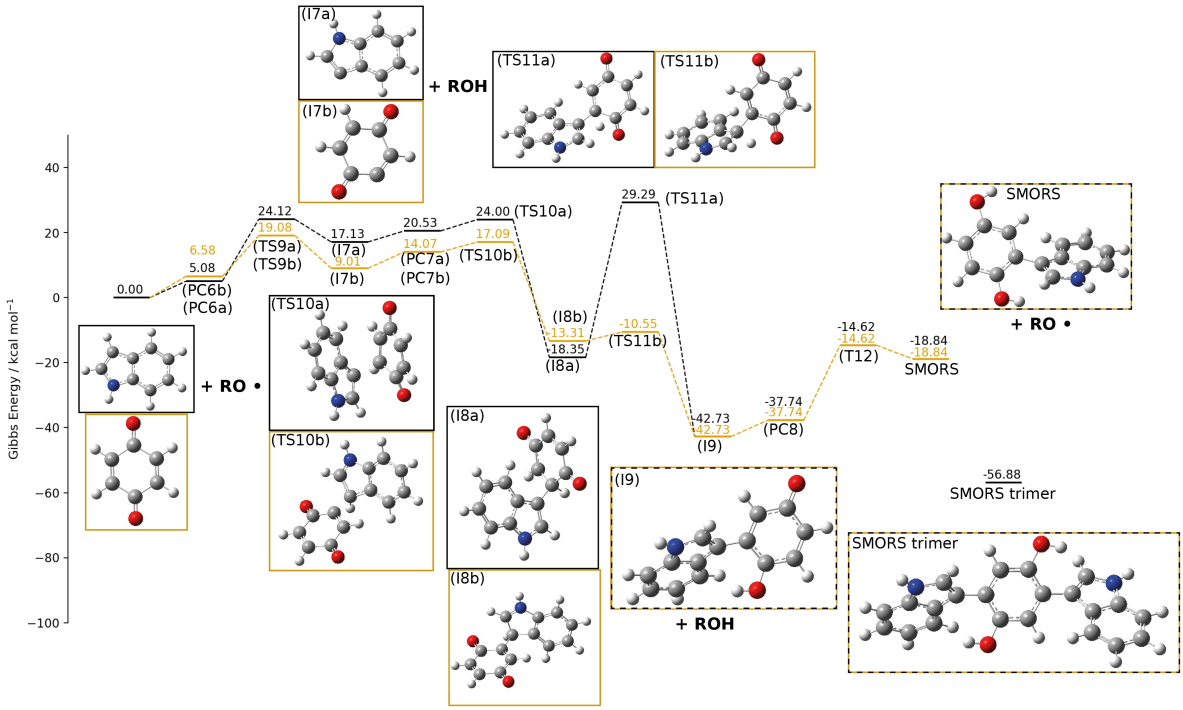

Figure 10: HAS step calculated at the B3LYP//cc-pVTZ n-dodecane PCM level of theory. The R group in this figure refers to an n-Dodecane moiety.

aromatization of the semiquinone compound **I9** via abstraction of hydrogen. Dodecanol produced in the first abstraction step (**0**→**TS9b**→**I7b**) was modelled as the species for hydrogen abstraction, allowing the efficiency of this radical propagation step to be assessed. The re-aromatization step with dodecanol proceeds endergonically (**I9**→**PC8**→**T12**→**SMORS**), showing the semiquinone compound **I9** is more stable than the dodecane hydroxy radical. However, overall the pathway to produce the final **SMORS** product is exergonic by -18.24 kcal mol^{-1} relative to the reactants state. This indicates this propagation cycle leading to SMORS is thermodynamically favorable. The stability of **I9** indicates that completion of the final re-aromatization step is disfavored. Formation of a SMORS trimer is likely given that the

SMORS trimer (Figure 12) is 14.15 kcal mol^{-1} more stable than **I9**. In this case an additional indole and dodecane hydroxy radical are consumed.

Our calculations show that SMORS can form under both acid catalyzed and oxidative conditions, in line with literature precedent.[64, 65] In order to investigate the formation of trimers under acid catalyzed and oxidative conditions a series of small scale testing was performed, as illustrated in the following section.

3.4. Flask Tests

Our calculations have shown that acid catalysis and/or oxidative conditions can lead to the formation of SMORS. To examine the effect of acids on the SMORS mechanism, two indole + phenol based model fuels were prepared, one containing acid forming dodecanethiol (IP-S) and one without (IP). The details of these tests are presented in the Supporting Information, in Section 4, along with a list of the molecular formula from (-)LCMS (negative mode LCMS), as well as the proposed structures. Each (-)LCMS peak was characterized in terms of species class by assigning the formula of the base peak to a species class. Subsequently, the areas associated with each class were grouped, allowing the % total area for each species class to be presented. This allows the relative abundance of each deposit class detected by (-)LCMS to be determined. The species classes and their associated percentage peak areas are presented in Figure 11a.

From (-)LCMS results, it is clear that the addition of thiol led to indole + sulfur oligomer formation, and suppressed the formation of SMORS. The heavy molecular weight materials corresponding to the IP-S surrogate contained compounds with molecular formulas associated with indole sulfonylation (**4**11b), arylated sulfonylation (**5**11b), and sulfenylation (**6**11b) reactions. These products have previously been detecting when indole and thiols have been combined under oxidative conditions.[62, 66, 54] A SMORS trimer (**1**11b) is directly observed in the IP surrogate deposit, suggesting that the SMORS process can proceed without the need of a strong acid catalyst, as weak carbxylic acids can still form from the autoxidation of bulk fuel.[67] This observation lends support to the HAS mechanism over an acid-catalyzed mechanism.

The formation of phenol dimers (**2**11b) in the sulfure-free IP surrogate deposit suggests that phenols are oxidized in the liquid phase. By contrast, no phenol oxidation products are observed in the sulfur containing IP-S surrogate. Instead, oxidized sulfur compounds form the largest proportion of the deposit. Co-elution of phenolic and oxidized sulfur compounds can be ruled out because phenolic compounds in IP elute at different retention times to oxidized sulfur compounds in IP-S (Tables 2 and 3 in the SI).

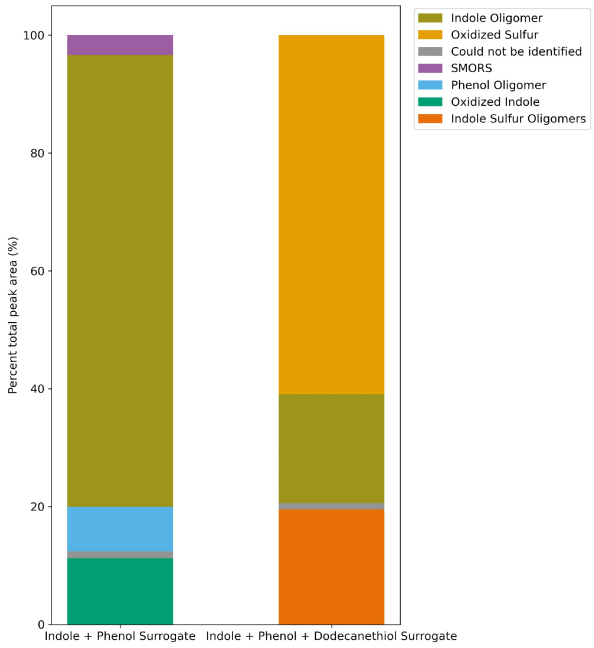

(a) (-)LCMS peak areas associated with the deposits generated from the n-dodecane $0.1\,\mathrm{mol\,L^{-1}}$ indole + phenol and $0.1\,\mathrm{mol\,L^{-1}}$ indole + phenol + dodecanethiol surrogates.

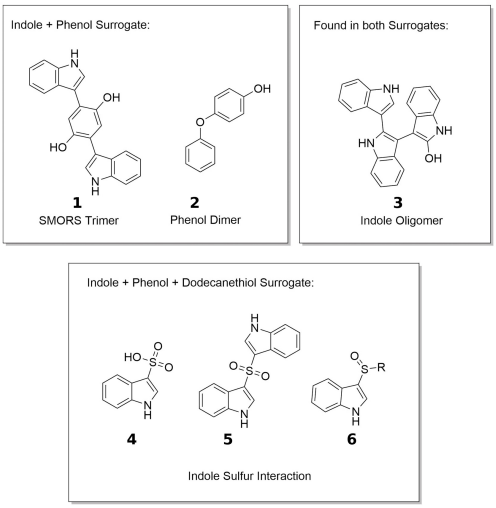

(b) Selected putative structures detected in the deposit. Detailed information of the deposit structures are present in Section 4 of the SI

Figure 11

3.5. Discussion and Implication for Fuels

The fact that different components in fuels interact with each other, either enhancing or slowing down deposit formation, is an uncontroversial idea. In fact, synergistic deposition enhancement between indole, phenol, and sulfur compounds in fuel has been observed in recent tests.[6] However, the mechanism by which this behind this synergistic behavior is still unclear. Our DFT and experimental results lead us to propose a modified SMORS mechanism. The first step in our mechanism is the oxidation of phenols (**1**) to quinones (**9**) are presented in Figure 3. The key weakness of the original SMORS proposal was the formation of quinones via a Russell Mechanism. Instead, we propose that quinones are produced via two main pathways, leading to a distribution of products. The first pathway, a two-step mechanism, involves the decomposition of the tetraperoxide (**5**) chain followed by hydrogen transfer. This leads to the production of one quinone (**7**), p-Chinole (**6**), and singlet oxygen (**8**). The second pathway, a single step-mechanism, involves the concerted decomposition of the tetraperoxide (**5**). This leads to the production of two quinones (**7**) and a hydrogen peroxide (**9**). The hydrogen peroxide (**9**) species is likely to undergo fission, yielding two HO$\cdot$ radicals, further propagating the chain-mechanism.

The second part of this modified SMORS mechanism is the coupling of quinone and indoles is proposed to occur via a HAS pathway, presented in Figure 13. The original EAS pathway, requires a stable, charged, σ-intermediate could not be located computationally in n-dodecane. Instead, a HAS pathway offers a route to a stable radical σ-intermediate via the attack of a quinone radical (**11**) on an indole (**13**). Quinone radicals could also attack other electron-rich fuel heterocyles like pyrroles and carbazoles, generalizing the scheme.

This is the first time a HAS pathway has been proposed as a route to fuel deposit formation. A HAS pathway also offers additional flexibility being a deposit formation which does not rely on free-radical termination to lead to C−C/C−O bond formation, and instead can be considered a propagation step. Beyond phenol and indole coupling, other fuel species could react to form via HAS reactions. A recent review focusing on HAS has shown these reactions can occur for both aromatic and heterocyclic compounds, including pyrrole and phenyls present in fuel. A particularly interesting facet of this review in relation to this work is the usage of SO_2 leaving groups for HAS coupling.[61] Indole containing SO_2/SO_3 leaving groups were directly observed

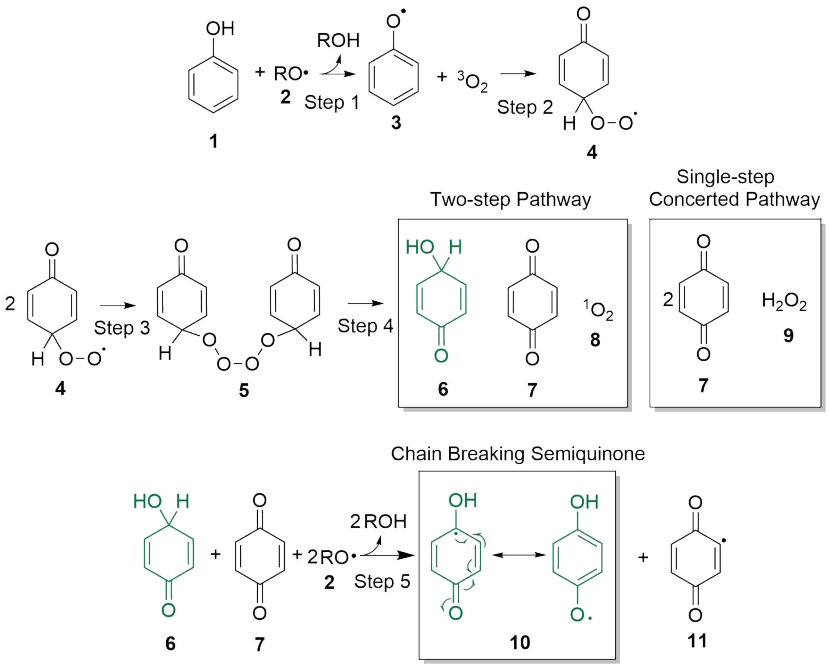

Figure 12: Modified SMORS mechanism: quinone production pathway

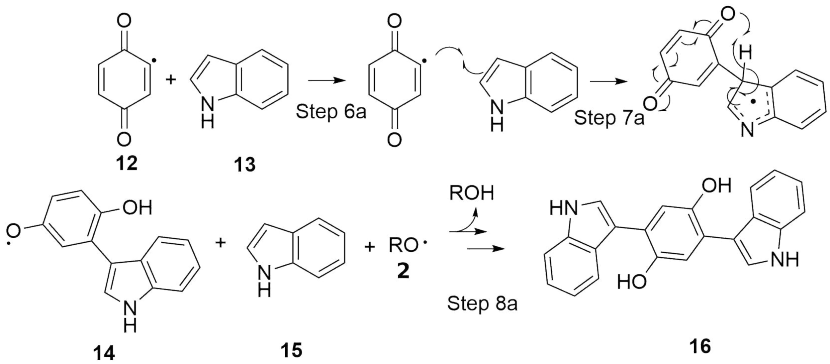

Figure 13: Modified SMORS mechanism: coupling mechanisms between indole and quinone

in the surrogate experiments (**4**,**5**11b).

The updated SMORS mechanism elucidated in this work will enable predictive aviation fuel stability mechanisms with higher accuracy. At present, existing predictive mechanisms contain no steps for nitrogen and phenol

interactions.[68, 1] This is largely due to the poor mechanistic understanding of the interactions between the species, despite the fact that deposition in conventional aviation fuels are highly correlated with nitrogen and phenol content.[7, 14] Additionally, a common weakness in existing pseudo-detailed mechanisms is implicit deposition steps. The work here presents an explicit generalized scheme for nitrogen and phenol deposit formation. The effect on kinetic and thermochemical parameters on the variations between different nitrogen species and different phenol structures using this generalized scheme can be studied, allowing for the eventual addition of explicit deposition steps in pseudo-detailed mechanisms.

4. Conclusions and Next Steps

The highly cited SMORS mechanism to explain phenol and fuel heteratom coupling in fuels was investigated by experimental and DFT methods. Several key modifications are made to the original proposed mechanism. First, in contrast to the proposed one-step Russell Mechanism, formation of quinone was shown to occur via a two-step mechanism. This occurs via the decomposition of a tetraperoxide, formed via the termination of two keto-peroxyl radicals, leading to two reactive hydroxy radicals and singlet oxygen. Hydroxy radicals then undergo a hydrogen transfer reaction to form quinone and a p-chinole, in contrast to the quinone, hydroquinone and triplet oxygen products in the original mechanism. The second important modification is the coupling step between quinone and electron-rich compounds. In apolar solvents, an electrophilic aromatic substitution (EAS) step was found to form unstable intermediates and was found to proceed with prohibitively high barriers. Instead, a homolytic aromatic substitution (HAS) mechanism was found to be the most likely pathway according to DFT calculated energies and experimental observations. Based on these findings, we propose a new modified SMORS pathway (Figures 12 and 13). Additionally, HAS reactions should begin to be explored as a new coupling pathway for fuel species.

5. Acknowledgements

References

[1] N. J. Kuprowicz, S. Zabarnick, Z. J. West, J. S. Ervin, Use of measured species class concentrations with chemical kinetic modeling for the

prediction of autoxidation and deposition of jet fuels, Energy and Fuels 21 (2) (2007) 530–544. doi:10.1021/ef060391o.

[2] R. N. Hazlett, J. A. Schreifels, W. M. Stalick, R. E. Morris, G. W. Mushrush, Distillate fuel insolubles: formation conditions and characterization, Energy and Fuels 5 (2) (1991) 269–273. doi:10.1021/ef00026a008.

[3] N. J. Kuprowicz, J. S. Ervin, S. Zabarnick, Modeling the liquid-phase oxidation of hydrocarbons over a range of temperatures and dissolved oxygen concentrations with pseudo-detailed chemical kinetics, Fuel 83 (13) (2004) 1795–1801. doi:10.1016/j.fuel.2004.03.013.
URL www.fuelfirst.com

[4] T. Jia, L. Pan, S. Gong, J. Xie, X. Wang, Y. Fang, J. J. Zou, X. Zhang, Mechanistic insights into the thermal deposition of highly thermal-stable jet fuel, Fuel 276 (May) (2020) 118100. doi:10.1016/j.fuel.2020.118100.
URL https://doi.org/10.1016/j.fuel.2020.118100

[5] J. W. Frankenfeld, W. F. Taylor, D. W. Brinkman, Storage stability of synfuels from oil shale. 1. general features of sediment formation in model fuel systems, Industrial and Engineering Chemistry Product Research and Development 22 (4) (1983) 608–614. doi:10.1021/i300012a018.

[6] S. Zabarnick, Z. J. West, L. M. Shafer, S. S. Mueller, R. C. Striebich, P. J. Wrzesinski, Studies of the role of heteroatomic species in jet fuel thermal stability: model fuel mixtures and real fuels, Energy and Fuels 33 (9) (2019) 8557–8565. doi:10.1021/acs.energyfuels.9b02345.

[7] L. M. Balster, S. Zabarnick, R. C. Striebich, L. M. Shafer, Z. J. West, Analysis of polar species in jet fuel and determination of their role in autoxidative deposit formation, Energy and Fuels 20 (6) (2006) 2564–2571. doi:10.1021/ef060275l.
URL https://pubs.acs.org/doi/abs/10.1021/ef060275l

[8] R. H. Clark, L. Smith, Further studies of the effects of polar compounds on the thermal stability of jet fuel, in: 3rd International Conference on Stability And Handling of Liquid Fuels, no. 2, 1988.

[9] B. Beaver, L. Gao, C. Burgess-Clifford, M. Sobkowiak, On the mechanisms of formation of thermal oxidative deposits in jet fuels. Are unified mechanisms possible for both storage and thermal oxidative deposit formation for middle distillate fuels?, Energy and Fuels 19 (4) (2005) 1574–1579. doi:10.1021/ef040090j.

[10] C. G. Kabana, S. Botha, C. Schmucker, C. Woolard, B. Beaver, Oxidative stability of middle distillate fuels. Part 1: Exploring the soluble macromolecular oxidatively reactive species (SMORS) mechanism with jet fuels, Energy and Fuels 25 (11) (2011) 5145–5157. doi:10.1021/ef200964z.

[11] M. Commodo, I. Fabris, C. P. T. Groth, Ö. L. Gülder, Analysis of aviation fuel thermal oxidative stability by electrospray ionization mass spectrometry (ESI-MS), Energy and Fuels 25 (5) (2011) 2142–2150. doi:10.1021/ef2002102.
URL https://pubs.acs.org/sharingguidelines

[12] R. Epping, S. Kerkering, J. T. Andersson, Influence of different compound classes on the formation of sediments in fossil fuels during aging, Energy and Fuels 28 (9) (2014) 5649–5656. doi:10.1021/ef501230c.

[13] K. M. Christison, R. M. Lorenz, L. Xue, O. D. Sparkman, Exploring the Molecular Origin of Jet Fuel Thermal Oxidative Instability through Statistical Analysis of Mass Spectral Data, Energy and Fuels 33 (2) (2019) 830–836. doi:10.1021/acs.energyfuels.8b03670.
URL https://pubs.acs.org/sharingguidelines

[14] M. Sobkowiak, J. M. Griffith, B. Wang, B. Beaver, Insight into the mechanisms of middle distillate fuel oxidative degradation. Part 1: On the role of phenol, indole, and carbazole derivatives in the thermal oxidative stability of fischer-tropsch/petroleum jet fuel blends, Energy and Fuels 23 (4) (2009) 2041–2046. doi:10.1021/ef8006992.
URL http://pubs.acs.org/doi/abs/10.1021/ef8006992

[15] D. R. Hardy, M. A. Wechter, Insoluble sediment formation in middle distillate diesel fuel: further evidence concerning the role of in situ fuel acidity, Fuel 69 (6) (1990) 720–724. doi:10.1016/0016-2361(90)90036-P.

[16] C. M. Parks, E. Alborzi, S. G. Blakey, A. J. Meijer, M. Pourkashanian, Density Functional Theory Calculations on Copper-Mediated Peroxide Decomposition Reactions: Implications for Jet Fuel Autoxidation, Energy and Fuels 34 (6) (2020) 7439–7447. doi:10.1021/acs.energyfuels.0c00918.

[17] S. Zabarnick, D. K. Phelps, Density functional theory calculations of the energetics and kinetics of jet fuel autoxidation reactions, Energy and Fuels 20 (2) (2006) 488–497. doi:10.1021/ef050348l.
URL https://pubs.acs.org/doi/full/10.1021/ef050348l?src=recsys

[18] C. M. Parks, A. J. Meijer, S. G. Blakey, E. Alborzi, M. Pourkashanian, Computational studies on the reactions of thiols, sulfides and disulfides with hydroperoxides. Relevance for jet fuel autoxidation, Fuel 316 (January) (2022) 123326. doi:10.1016/j.fuel.2022.123326.
URL https://doi.org/10.1016/j.fuel.2022.123326

[19] E. Alborzi, M. R. Dwyer, C. M. , A. Sheikhansari, D. C. Mielczarek, M. Zanganeh, A. J. Meijer, S. G. Blakey, M. Pourkashanian, Construction of a reduced chemical kinetic mechanism for autoxidation of n-paraffinic solvent – A model for aviation fuel, Fuel 294 (January) (2021) 120170. doi:10.1016/j.fuel.2021.120170.
URL https://doi.org/10.1016/j.fuel.2021.120170

[20] P. Hohenberg, W. Kohn, Inhomogenous Electron Gas, Physical Review 136 (1964) 864–871. doi:10.1007/BF01198136.
URL https://journals.aps.org/pr/pdf/10.1103/PhysRev.136.B864

[21] M. J. Frisch, G. W. Trucks, H. B. Schlegel, G. E. Scuseria, M. A. Robb, J. R. Cheeseman, G. Scalmani, V. Barone, B. Mennucci, G. A. Petersson, H. Nakatsuji, M. Caricato, X. Li, H. P. Hratchian, A. F. Izmaylov, J. Bloino, G. Zheng, J. L. Sonnenberg, M. Hada, M. Ehara, K. Toyota, R. Fukuda, J. Hasegawa, M. Ishida, T. Nakajima, Y. Honda, O. Kitao, H. Nakai, T. Vreven, J. A. Montgomery, Jr., J. E. Peralta, F. Ogliaro, M. Bearpark, J. J. Heyd, E. Brothers, K. N. Kudin, V. N. Staroverov, R. Kobayashi, J. Normand, K. Raghavachari, A. Rendell, J. C. Burant, S. S. Iyengar, J. Tomasi, M. Cossi, N. Rega, J. M. Millam, M. Klene, J. E.

Knox, J. B. Cross, V. Bakken, C. Adamo, J. Jaramillo, R. Gomperts, R. E. Stratmann, O. Yazyev, A. J. Austin, R. Cammi, C. Pomelli, J. W. Ochterski, R. L. Martin, K. Morokuma, V. G. Zakrzewski, G. A. Voth, P. Salvador, J. J. Dannenberg, S. Dapprich, A. D. Daniels, Ö. Farkas, J. B. Foresman, J. V. Ortiz, J. Cioslowski, D. J. Fox, Gaussian 09 Revision E.01, gaussian Inc. Wallingford CT 2009 (2009).

[22] A. D. Becke, Density-functional thermochemistry. III. The role of exact exchange, The Journal of Chemical Physics 98 (7) (1993) 5648–5652. doi:10.1063/1.464913.

[23] S. Grimme, S. Ehrlich, L. Goerigk, Effect of the damping function in dispersion corrected density functional theory, Journal of computational chemistry 32 (7) (2011) 1456–1465.

[24] S. Miertuš, E. Scrocco, J. Tomasi, Electrostatic interaction of a solute with a continuum. a direct utilizaion of ab initio molecular potentials for the prevision of solvent effects, Chemical Physics 55 (1) (1981) 117–129.

[25] T. H. Dunning Jr, Gaussian basis sets for use in correlated molecular calculations. i. the atoms boron through neon and hydrogen, The Journal of chemical physics 90 (2) (1989) 1007–1023.

[26] S. Grimme, Supramolecular binding thermodynamics by dispersion-corrected density functional theory, Chemistry–A European Journal 18 (32) (2012) 9955–9964.

[27] R. F. Ribeiro, A. V. Marenich, C. J. Cramer, D. G. Truhlar, Use of solution-phase vibrational frequencies in continuum models for the free energy of solvation, The Journal of Physical Chemistry B 115 (49) (2011) 14556–14562.

[28] R. Paton, Goodvibes (2016).
URL https://github.com/patonlab/GoodVibes

[29] C. Riplinger, F. Neese, An efficient and near linear scaling pair natural orbital based local coupled cluster method, The Journal of chemical physics 138 (3) (2013) 034106.

[30] C. Riplinger, B. Sandhoefer, A. Hansen, F. Neese, Natural triple excitations in local coupled cluster calculations with pair natural orbitals, The Journal of chemical physics 139 (13) (2013) 134101.

[31] C. Riplinger, P. Pinski, U. Becker, E. F. Valeev, F. Neese, Sparse maps—a systematic infrastructure for reduced-scaling electronic structure methods. ii. linear scaling domain based pair natural orbital coupled cluster theory, The Journal of chemical physics 144 (2) (2016) 024109.

[32] M. Saitow, U. Becker, C. Riplinger, E. F. Valeev, F. Neese, A new near-linear scaling, efficient and accurate, open-shell domain-based local pair natural orbital coupled cluster singles and doubles theory, The Journal of chemical physics 146 (16) (2017) 164105.

[33] Y. Guo, C. Riplinger, U. Becker, D. G. Liakos, Y. Minenkov, L. Cavallo, F. Neese, Communication: An improved linear scaling perturbative triples correction for the domain based local pair-natural orbital based singles and doubles coupled cluster method [dlpno-ccsd (t)], The Journal of chemical physics 148 (1) (2018) 011101.

[34] F. Neese, F. Wennmohs, U. Becker, C. Riplinger, The ORCA quantum chemistry program package, Journal of Chemical Physics 152 (22) (2020). doi:10.1063/5.0004608.
URL https://doi.org/10.1063/5.0004608

[35] M. Dwyer, S. Blakey, E. Alborzi, A. Meijer, The role of hydrocarbon composition on the thermal stability of aviation fuels, in: IASH 2017, the 15th International Symposium on Stability, Handling and Use of Liquid Fuels Rome,, no. September, 2017. doi:10.1021/ja111674c.

[36] D. Min, J. Boff, Chemistry and reaction of singlet oxygen in foods, Comprehensive reviews in food science and food safety 1 (2) (2002) 58–72.

[37] B. Dellinger, S. Lomnicki, L. Khachatryan, Z. Maskos, R. W. Hall, J. Adounkpe, C. McFerrin, H. Truong, Formation and stabilization of persistent free radicals, Proceedings of the Combustion Institute 31 I (1) (2007) 521–528. doi:10.1016/j.proci.2006.07.172.

[38] L. Jones, N. C. Li, Ageing of SRC II middle distillate from Illinois No. 6 coal, Fuel 62 (10) (1983) 1156–1160. doi:10.1016/0016-2361(83)90057-1.

[39] H. Shadnia, J. S. Wright, Understanding the toxicity of phenols: Using quantitative structure-activity relationship and enthalpy changes to discriminate between possible mechanisms, Chemical Research in Toxicology 21 (6) (2008) 1197–1204. doi:10.1021/tx800058r.

[40] M. Michalík, P. Poliak, V. Lukeš, E. Klein, From phenols to quinones: Thermodynamics of radical scavenging activity of para-substituted phenols, Phytochemistry 166 (July) (2019) 112077. doi:10.1016/j.phytochem.2019.112077.
URL https://doi.org/10.1016/j.phytochem.2019.112077

[41] E. T. Denisov, I. B. Afanas' ev, Oxidation and antioxidants in organic chemistry and biology, CRC press, 2005.

[42] G. A. Russell, Deuterium-isotope effects in the autoxidation of aralkyl hydrocarbons. mechanism of the interaction of peroxy radicals1, Journal of the American Chemical Society 79 (14) (1957) 3871–3877.

[43] R. Lee, G. Gryn'Ova, K. U. Ingold, M. L. Coote, Why are: Sec -alkylperoxyl bimolecular self-reactions orders of magnitude faster than the analogous reactions of tert -alkylperoxyls? the unanticipated role of CH hydrogen bond donation, Physical Chemistry Chemical Physics 18 (34) (2016) 23673–23679. doi:10.1039/c6cp04670c.

[44] K. Adamic, J. A. Howard, K. U. Ingold, Absolute rate constants for hydrocarbon autoxidation. XVI. Reactions of peroxy radicals at low temperatures, Canadian Journal of Chemistry 47 (20) (1969) 3803–3808. doi:10.1139/v69-634.
URL www.nrcresearchpress.com

[45] A. R. Smith, S. Di Muzio, F. Ramondo, G. Meloni, Peroxy self-reaction leading to the formation of furfural, Physical Chemistry Chemical Physics 21 (20) (2019) 10228–10237. doi:10.1039/c8cp07571a.

[46] J. Howard, J. Bennett, The self-reaction of sec-alkylperoxy radicals: a kinetic electron spin resonance study, Canadian Journal of Chemistry 50 (14) (1972) 2374–2377.

[47] G. Mendenhall, E. Quinga, Deuterium isotope cage effects in the dismutation of alkoxyl radicals. significance for the mode of alkylperoxyl termination, International journal of chemical kinetics 17 (11) (1985) 1187–1190.

[48] E. Quinga, G. Mendenhall, Chemiluminescence from hyponitrite esters. excited triplet states from dismutation of geminate alkoxyl radical pairs, Journal of the American Chemical Society 105 (21) (1983) 6520–6521.

[49] J. Helberg, D. A. Pratt, Autoxidation vs. antioxidants-the fight for forever, Chemical Society Reviews 50 (13) (2021) 7343–7358. doi:10.1039/d1cs00265a.

[50] M. Dwyer, Investigating The Role Of Aviation Fuels Hydrocarbon Chemistry On Its Autoxidation, Ph.D. thesis, University of Sheffield (2019).

[51] T. Jia, M. Zhao, L. Pan, C. Deng, J. J. Zou, X. Zhang, Effect of phenolic antioxidants on the thermal oxidation stability of high-energy–density fuel, Chemical Engineering Science 247 (2022) 117056. doi:10.1016/j.ces.2021.117056.
URL https://doi.org/10.1016/j.ces.2021.117056

[52] R. E. Gawley, A proposal for (slight) modification of the hughes-ingold mechanistic descriptors for substitution reactions, Tetrahedron letters 40 (23) (1999) 4297–4300.

[53] S. L. Matlow, G. W. Wheland, Orientation in Aromatic Substitution: A Theoretical Study of the Competition between Groups, Journal of the American Chemical Society 77 (13) (1955) 3653–3655. doi:10.1021/ja01618a073.

[54] Hongchang, Sulfonation mechanism of benzene with SO3 in sulfuric acid or oleum or aprotic solvent: Obeying the transition state theory via a trimolecular electrophilic substitution clarified by density functional theory calculation, Computational and Theoretical Chemistry 1112 (2017) 111–122. doi:10.1016/j.comptc.2017.04.012.
URL http://dx.doi.org/10.1016/j.comptc.2017.04.012

[55] T. Stuyver, D. Danovich, F. De Proft, S. Shaik, Electrophilic Aromatic Substitution Reactions: Mechanistic Landscape, Electrostatic and

Electric-Field Control of Reaction Rates, and Mechanistic Crossovers, Journal of the American Chemical Society 141 (24) (2019) 9719–9730. doi:10.1021/jacs.9b04982.

[56] M. C. Pirrung, L. Deng, Z. Li, K. Park, Synthesis of 2, 5-dihydroxy-3-(indol-3-yl) benzoquinones by acid-catalyzed condensation of indoles with 2, 5-dichlorobenzoquinone, The Journal of Organic Chemistry 67 (24) (2002) 8374–8388.

[57] M. G. Corradini, C. Costanini, G. Prota, T. Schultz, Acid-catalyzed reactions of indoles with 1, 4-quinones., ChemInform 20 (33) (1989).

[58] S. Baena-Zambrana, S. L. Repetto, C. P. Lawson, J. K. Lam, Behaviour of water in jet fuel - A literature review, Progress in Aerospace Sciences 60 (2013) 35–44. doi:10.1016/j.paerosci.2012.12.001.

[59] S. P. Heneghan, S. Zabarnick, Oxidation of jet fuels and the formation of deposit, Fuel 73 (1) (1994) 35–43. doi:10.1016/0016-2361(94)90185-6.
URL https://www.sciencedirect.com/science/article/pii/0016236194901856

[60] M. Gurry, F. Aldabbagh, A new era for homolytic aromatic substitution: Replacing Bu3SnH with efficient light-induced chain reactions, Organic and Biomolecular Chemistry 14 (16) (2016) 3849–3862. doi:10.1039/c6ob00370b.

[61] W. R. Bowman, J. M. Storey, Synthesis using aromatic homolytic substitution—recent advances, Chemical Society Reviews 36 (11) (2007) 1803–1822. doi:10.1039/b605183a.

[62] S. Liu, F. Zhao, X. Chen, G. J. Deng, H. Huang, Aerobic oxidative functionalization of indoles, Advanced Synthesis and Catalysis 362 (18) (2020) 3795–3823. doi:10.1002/adsc.202000285.

[63] M. Nonella, A Generalized Resonance Model for Substituted 1,4-Benzoquinones, Journal of Physical Chemistry A 103 (35) (1999) 7069–7075. doi:10.1021/jp9907847.

[64] J. S. Yadav, B. V. Reddy, T. Swamy, InBr3-Catalyzed Conjugate Addition of Indoles to p-Quinones: An Efficient Synthesis of 3-Indolylquinones, Synthesis 44 (1) (2004) 106–110. doi:10.1055/s-2003-44364.

[65] J. Stejskal, P. Bober, M. Trchová, J. Horský, Z. Walterová, S. K. Filippov, T. Plachý, M. Mrlík, Oxidation of pyrrole with: P -benzoquinone to semiconducting products and their application in electrorheology, New Journal of Chemistry 42 (12) (2018) 10167–10176. doi:10.1039/c8nj01283k.

[66] F. Takahashi, K. Nogi, H. Yorimitsu, Catalytic inter- and intramolecular coupling of aryl sulfones, Phosphorus, Sulfur and Silicon and the Related Elements 194 (7) (2019) 742–745. doi:10.1080/10426507.2019.1603232.
URL https://doi.org/10.1080/10426507.2019.1603232

[67] B. D. Boss, R. N. Hazlett, Oxidation of hydrocarbons in the liquid phase: n-dodecane in a borosilicate glass chamber at 200 °C, Canadian Journal of Chemistry 47 (1969) 4176–4182.

[68] Z. Liu, S. Tang, Z. Li, Z. Qin, S. Yuan, L. Wang, L. Wang, X. Zhang, G. Liu, An improved kinetic model for deposition by thermal oxidation of aviation hydrocarbon fuels, Fuel 258 (June) (2019) 116139. doi:10.1016/j.fuel.2019.116139.
URL https://doi.org/10.1016/j.fuel.2019.116139

Mechanistic Investigation Into The Formation of Insolubles in Bulk Fuel Jet Fuel Using Quantum Chemical and Experimental Techniques

Charlie Adams[a], Ehsan Alborzi[a], Anthony J.H.M. Meijer[b], Kevin J. Hughes[a], Mohamed Pourkashanian[a]

[a] *Department of Mechanical Engineering The University of Sheffield, S3 7HF, UK*
[b] *Department of Chemistry The University of Sheffield, S3 7HF, UK*

Abstract

The SMORS mechanism describing the formation of insoluble material in bulk jet fuel was investigated using density functional and experimental techniques. The first part of the SMORS mechanism, the formation of quinones from the oxidation of indigenous fuel phenols, was shown to proceed via two possible pathways. First, a single-step pathway yielding two quinones and a hydrogen peroxide. Secondly, a two-step pathway yielding a quinone, p-chinole and singlet oxygen. The second step of the SMORS mechanism, the reaction of quinones with electron-rich heterocyles in fuels, was shown to proceed via a homolytic aromatic substitution pathway. These findings, allow us to propose a modified SMORS mechanism, built on our enhanced mechanistic understanding of fuel deposit formation.

1. Introduction

Liquid-phase jet fuel thermal oxidative degradation in conventional fuels is largely driven by minor heteroatomic species.[1] The process of jet fuel thermal degradation can be split into three main stages: 1) autoxidation of the bulk fuel yielding oxidized species, 2) agglomeration of oxidized components to high molecular weight species, 3) formation of insolubles.[2] There is a better understanding of step 1 than step 2, and this is reflected in the existing pseudo-detailed mechanisms for deposition, where there are more steps representing autoxidation reactions.[3, 1, 4]

*Charlie Adams
**Ehsan Alborzi
Email addresses: bismuthadams@sheffield.ac.uk (Charlie Adams), e.alborzi@sheffield.ac.uk (Ehsan Alborzi), a.meijer@sheffield.ac.uk (Anthony J.H.M. Meijer)

To understand the agglomeration and insoluble formation processes in more detail, researchers have taken the approach of correlating initial polar concentrations with mass of deposit.[5, 6, 7] Phenols and electron-rich nitrogen compounds, indoles and carbazoles, were found to correlate well with mass of deposit.[7] In fact, phenol and electron-rich nitrogen compounds have been found to interact synergistically to enhance deposit formation in fuels.[6, 8] To explain this synergistic effect, Beaver *et al.* proposed the Soluble Macromolecular Oxidatively Reactive Species (SMORS) mechanism.[9] The SMORS mechanism was originally based on work by Hardy and Wechter. Hardy and Wechter identified nitrogen and oxygen containing deposit precursors using methanol extraction, where Beaver *et al.* proposed these precursors to form from quinone-aromatic coupling species. Several articles have subsequently used this mechanism to explain observed deposition effects,[10, 11, 12, 13] but none have explored the SMORS mechanism in depth.

The original SMORS mechanism proposed by Beaver *et al.* is described in detail in the following reference[9] and in Figure 1. It relies on the formation of electrophilic quinones from the oxidation of phenol. These quinones are then proposed to undergo electrophilic aromatic substitution reactions (EAS) with electron-rich heteroatomic compounds in fuel.[14] Using indole as a model for nitrogen heterocycle leads to the formation of a 3-indolyl hydroquinone. The EAS product between quinone and nitrogen heterocycles is proposed to undergo further EAS steps to successively larger structures, ultimately forming insoluble particles in fuel.[10]

In recent years, density functional theory (DFT) has become an increasingly popular tool to investigate thermal oxidative reactions in fuel.[16, 17, 18, 19] DFT rests upon the assumption that the electron density in an atom/molecule is related to the ground state energy of the system, which in turn can be used to calculate thermochemical and kinetic parameters of reaction systems.[20] Early work by Zabarnick *et al.* used the B3LYP//6-31G(d) level of theory to investigate X−H bond dissociation energies of various fuel heteroatoms to understand their chain-breaking properties.[17] Building on these methods, Parks et al. used the B3LYP//cc-pVTZ level of theory to propose a copper catalyzed hydroperoxide decomposition cycle.[16] Further work by Parks et al. successively elucidated thermally oxidation pathways of a variety of sulfur classes.[18]

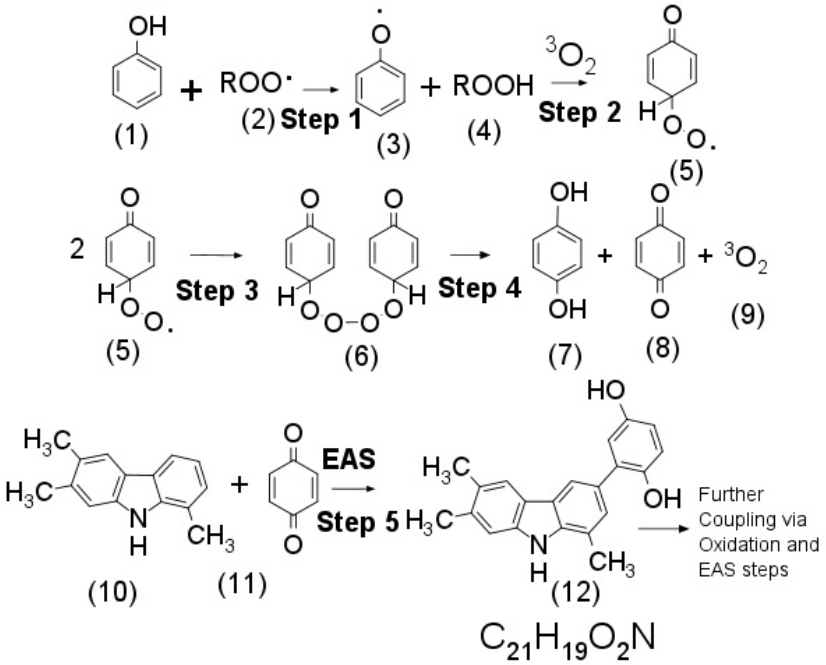

Figure 1: SMORS mechanism as described in reference[9]. The compound **(12)** is found as an extract in Hardy and Wechter's original paper.[15]

It is the aim of this work to investigate the proposed SMORS mechanism at a molecular level using DFT methods, while proposing alternative pathways where appropriate. Additionally, our DFT calculations will enhance the understanding of the SMORS mechanism itself, and allow us to propose alternative pathways. Moreover, a greater mechanistic understanding of the SMORS mechanism will eventually lead to enhanced predictive capabilities in the form of pseudo-detailed mechanisms.

2. Materials and Methods

2.1. Computational Details

All calculations were performed in Gaussian09 (E.01) using the B3LYP functional.[21][22] Grimme's DFT-D3(BJ) dispersion correction was applied to all the calculations to account for long-range effects.[23] A PCM solvation model, with *n*-dodecane as the chosen solvent, was selected to replicate the hydrocarbon bulk.[24] The basis set chosen was cc-pVTZ on an *ultrafine* grid,

this basis set adds polarization functions, thus orbital hybridization can be taken into account.[25] Transition states were optimized using the QST1/3 method depending on the reaction studied. All transition states were verified by the presence of one imaginary frequency corresponding to the saddle point. Additionally, intrinsic reaction coordinate (IRC) calculations were performed to verify the transition state corresponded to the expected reactants and products. Unrestricted (broken symmetry) calculations were performed on open-shell systems, where the HOMO and LUMO were mixed (`guess=mix` option). Entropy values were corrected using the GoodVibes script, which employs a quasi-harmonic correction corrected at 298 K.[26, 27, 28] The quinone oxidation pathway in Section 3.2 was further validated with single point DLPNO-CCSD(T)[29, 30, 31, 32, 33] calculations using the ORCA quantum chemistry package.[34] DLPNO-CCSD(T) allows near CCSD(T) accurate calculations at a fraction of the cost by identifying electron pairs with significant contributions to correlation energy, where the correlation energies for the other pairs are obtained at the MP2 level of theory.

2.2. Surrogate Fuels

The details of the experimental setup can be found in the supporting information (Section 4).

3. Results and Discussion

In this section we will present the DFT calculations for each step of SMORS, in conformity with reference.[9]

3.1. Formation of the Keto-Peroxyl Radical

The first set of calculations was focused on the generation of keto peroxyl radical, indicated as (**P1**) in Figure 2. In the generalized SMORS reaction scheme, the first step involves the abstraction of a hydrogen atom from a phenol (representing an indigenous antioxidant) by a hydroxy radical ROO$\cdot$. As shown in Figure 2, the Gibbs free energy barrier corresponding to the transition state of this reaction (**TS1**) is $\Delta_{\ddagger}G$=+12.65 kcal mol^{-1}; the overall reaction is slightly endergonic, with a $\Delta_r G$(ROO$\cdot$)= +0.40 kcal mol^{-1}.

Comparing the hydrogen abstraction step for the reaction between phenol and different n-dodecane fuel radical classes (R$\cdot$, RO$\cdot$, ROO$\cdot$)[1], the RO$\cdot$ pathway provides the lowest barriers. The calculated values for each pathway

Species	$\Delta_{\ddagger}S$ (kcal mol^{-1}K^{-1})	$\Delta_{\ddagger}H$ (kcal mol^{-1})	$\Delta_{\ddagger}G$ (kcal mol^{-1})	$\Delta_{r}S$ (kcal mol^{-1}K^{-1})	$\Delta_{r}H$ (kcal mol^{-1})	$\Delta_{r}G$ (kcal mol^{-1})
R $\cdot$	-2.749E-02	8.24	9.97	-1.440E-03	-18.88	-17.98
RO $\cdot$	-2.037E-02	0.29	1.32	1.24E-03	-3.31	-20.79
ROO $\cdot$	-2.327E-03	8.94	10.40	9.00E-06	0.40	0.40

Table 1: Calculated energy change of reaction $\Delta_{\ddagger}$ and formation Δ_r values for reaction of phenol with different dodecane fuel radicals calculated at the B3LYP-D3//cc-pVTZ n-dodecane PCM level of theory. Enthalpy values are corrected with GoodVibes at 298K. All $\Delta_{\ddagger}$ values are calculated from stable pre-collision complexes located from an IRC calculation.

associated for each radical class are presented in Table 1 and the comparison for each pathway is shown in Figure 2. The higher associated barriers $\Delta_{\ddagger}G$ for the R $\cdot$ and ROO $\cdot$ species compared to RO $\cdot$ are likely due to the higher level of distortion associated with these barriers. Energies of formation $\Delta_r G$ for the radical classes go from highest to lowest RO $\cdot$ $>$ R $\cdot$ $>$ ROO $\cdot$. The ability of the electron-rich oxygens to share spin density with the ring can justify the lower peroxyl radical reactivity, leading to enhanced radical stability. Whereas the alkyl radical is stabilized solely by the inductive effects from the adjacent carbons.[35]

The next step in the SMORS mechanism is the reaction of dissolved oxygen with the resulting phenoxy radical. In order to study this step computationally, triplet oxygen was selected for the calculation, because of its higher stability and commonality in nature.[36] Our results indicate that the reaction between dissolved oxygen and the phenoxy radical is endothermic, with a $\Delta_r G$=+15.23 kcal/mol. The transition state with a barrier of $\Delta_r G$=+21.50 kcal/mol was identified for this reaction (**TS2** in Figure 2), which is in good agreement with the previous work.[37] Overall, the formation of keto-peroxyl radical (**P1** in Figure 2) is endergonic, indicating that high temperatures would be needed for this species to form. However, the exergonicity of the reactions of phenol with R $\cdot$ and RO $\cdot$ more than compensates for this, making the hydrogen abstraction using R $\cdot$ or RO $\cdot$ exergonic overall

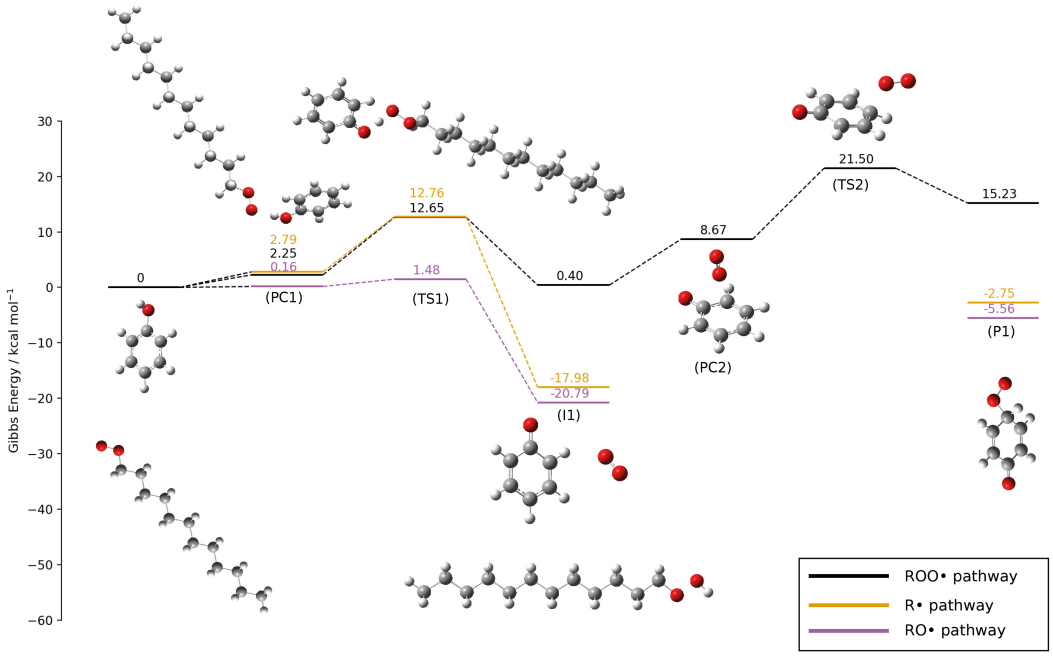

Figure 2: Potential energy surface (Gibbs energy) for the formation of the keto peroxyl radical calculated at the B3LYP-D3//cc-pVTZ level of theory using *n*-dodecane (PCM) as a solvent.

and making these reactions more favorable than the reaction with ROO· Nevertheless, the concentration of these chain-carrying radicals will be important too, with ROO· being primary chain carriers due to their higher concentration.[2]

3.2. Formation of Quinones

The next step proposed in the SMORS mechanism is the chain termination of two keto peroxyl radicals, resulting in the formation of a quinone, a hydroquinone and oxygen. Quinones have been found to form from substituted and unsubstituted phenols in fuels under oxidative conditions.[38, 4] The formation of quinones from phenols is universally found to occur *via* a termination step.[39, 40, 41] In the SMORS mechanism proposed by Beaver *et al.*

it has been suggested that this step is likely to proceed with the formation of a tetraperoxide (ROOOOR) intermediate, formed from the recombination of two keto-peroxyl radicals. Beaver *et al.* then propose quinones are formed by the decomposition of the ROOOOR via a Russell Mechanism decomposition, leading to the final products.[42] However, our DFT calculations suggest that this is unlikely. The final SMORS species are 104.89 kcal mol^{-1} (indicated as the red level in Figure 3) lower than the starting state of keto-peroxyl radicals. However, it is highly unlikely that the α hydrogen (labelled as 1 in Figure 3) would be able to move to the para-oxygen (labelled as 2 in Figure 3), given that the distance of 4.75 Å is prohibitive to hydrogen transfer. Indeed no transition state was found for this hydrogen transfer.

Because the termination of two radicals is unlikely, the production of keto-peroxyl radicals and subsequent tetroxide formation in competition with *n*-dodecane autoxidation and other phenol H-abstraction pathways was explored using a pseudo-detailed mechanism. The details of the pseudo-detailed mechanism are presented in Section 5. The final concentrations of the species from our pseudo-detailed mechanism is presented in Table 5. Despite the competing steps, the formation of the tetroxide is still competitive with the other autoxidation and hydrogen abstraction steps, with the concentrations greater or similar to *n*-dodecane autoxidation products found.

Alternative to the proposed oxidation products in reference [9], several pathways yielding a p-chinole (**a**), quinone (**b**), and singlet oxygen (**c**). These are shown as **P2a,b,d** in Figure 3. Additionally, a pathway yielding two quinones (**a**) and hydrogen peroxide (**d**) were found (**P2c** in Figure 3).

The first step is the formation of the tetraperoxide. A barrier of 13.36 kcal mol^{-1} (**TS3**) for peroxyl radical recombination and the formation of the tetraperoxide (**I2**) was found in our calculations, which is similar to the previous work on peroxyl radicals.[43]. Furthermore, the formation of the tetraperoxide (**I2**) is endergonic, with a Gibbs energy +8.05 kcal mol^{-1} above the separated species. This can be attributed to the instability of the linear ROOOOR structure.[44] It is worth mentioning that no stable ROOOOR species was found on the triplet surface, which is in agreement with previous work.[45]

The decomposition of ROOOOR can proceed through several pathways which are discussed here. First, a modified Russell Mechanism pathway was explored,

leading to the formation of quinone (**I2** → **TS4a** → **P2a,b,d**) However, the Russell mechanism pathway was found to have a high Gibbs free energy barrier of $\Delta_{\ddagger}G$=+34.91 kcal mol^{-1} . Such a high energy barrier indicates that the Russell mechanism is unlikely to contribute significantly to quinone formation, when compared to other calculated pathways in this section. We note that experimental work has found little evidence for the Russell Mechanism[42] in peroxyl self-reactions producing ROH, RCHO and O_2 products.[46, 47, 48]

Given that the Russell Mechanism decomposition of the tetraperoxide was found to have a large free energy barrier, we considered other pathways. As a consequence, an exergonic single-step channel was identified (**I2** → **TS4c** → **P2c**), yielding a two quinones and a hydrogen peroxide **P2c**. First, the tetraperoxide decomposes via **T4c** ($\Delta_{\ddagger}G$=10.87 kcal mol^{-1}), predicting a simultaneous transfer of two α-hydrogens to two oxygens in the ROOOOR chain and the cleavage of two O-O bonds. The IRC calculation for this transition state can be found in Figure 1 in the SI. Production of hydrogen peroxide from peroxyl self-reactions has been detected in previous work.[41] But, to the best of our knowledge, this is the first time a concerted hydrogen peroxide production step has been located.

A second pathway consists of a two-step channel yielding a quinone, p-chinole, and singlet oxygen species was identified (**I2** → **TS4b** → **I3b** → **TS5b** → **P2a,b,d**). This includes a transition state **TS4b** ($\Delta_{\ddagger}G$=25.27 kcal mol^{-1}) involving a simultaneous cleavage of one O-O and transfer of an α-hydrogen to an oxygen. The resultant intermediate formed (**I3b**) is a stable hydrotrioxide (ROOOH) species hydrogen bonded to a quinone species ($\Delta_r G$=−51.58 kcal/mol). Subsequently, the hydrotrioxide species can decompose via a transition state **TS5b** of $\Delta_{\ddagger}G$=44.26 kcal/mol, characterized by a four membered cyclic structure. This level of energy barrier is in agreement with the previous work.[45, 43] The high barriers for **TS4b** and **TS5b** show that this channel is prohibitive for the production of quinone.

Finally, a further two-step channel leading to a quinone, p-Chinole and singlet oxygen species was identified (**I2** → **I3d** → **TS5d** → **P2a,b,d**). The first step in this pathway is the exergonic decomposition of the ROOOOR species ($\Delta_r G$=-3.27 kcal mol^{-1}), yielding two hydroxy radicals and a singlet oxygen.[49, 50] In a related work, a potential energy surface scan of the CCSD//6-31G(d) level of theory on this step with ethane peroxyl radicals in-

dicates that this is a barrierless process.[43] In our case also, no transition state was found. Following the decomposition of the tetraperoxide, an α-hydrogen from one peroxyl radical is then transferred linearly to the other peroxyl O atom, yielding **P2a,b,d** with an energy barrier of $\Delta_{\ddagger}G$=+18.84 kcal mol^{-1} corresponding to **TS5d** in Figure 3.

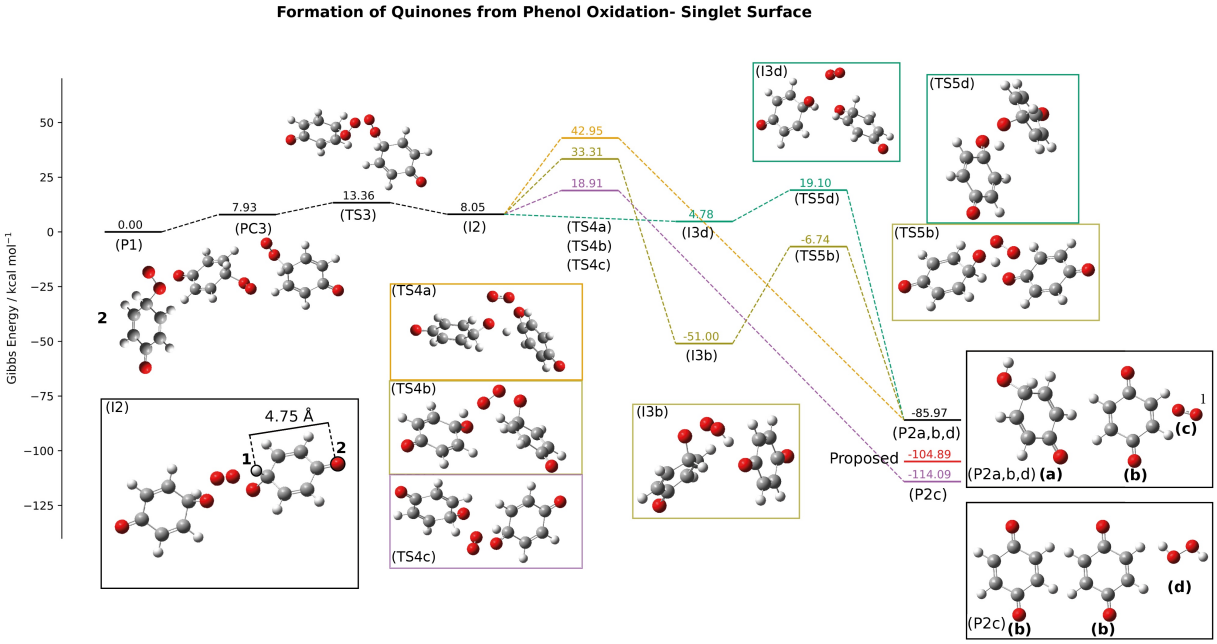

Figure 3: Potential energy surface (Gibbs energy) of the keto-peroxyl radical yielding quinones on the singlet surface, calculated at the B3LYP-D3//cc-pVTZ using n-dodecane (PCM) as a solvent. The red level indicates energy of the proposed quinone oxidation products, where no pathway could be found to form them.

To identify competing oxidation pathways, other non-quinone producing pathways were considered, as shown in Figure 4. On the singlet surface, an exergonic aromatic substitution pathway is identified, leading to ROOR species and singlet oxygen (**P1** $\rightarrow$ **PC4a** $\rightarrow$ **TS6a** $\rightarrow$ **P4**), without producing quinone. In this pathway, at **TS6a** a rocking movement of the peroxyl radical towards an α-carbon on the other peroxyl radical is observed. This is in association

with the simultaneous cleavage of a C−O liberating singlet oxygen is observed. However, the high energy barrier of **TS6a** ($\Delta_{\ddagger}G$=+59.46 kcal mol^{-1}) means that the termination of ROOOOR (**I2**) via **TS3** is strongly preferred, suggesting this pathway can be excluded.

On the triplet surface, an exergonic pathway was identified, which leads to the production of two hydroxy radicals and a triplet oxygen (**P1** → **PC4b** → **TS6b** → **P3**). The first step of this pathway is the formation of a dimeric pre-reaction complex (**PC4b**). Following **PC4b**, a high energy transition state (**TS6b**) was characterized via the simultaneous scission of O−O bonds on each peroxyl radical and the formation of new O−O bonds between terminal oxygens. The very high barrier associated with **TS6b** ($\Delta_{\ddagger}G$=+51.49 kcal/mol) means that this pathway will not proceed beyond **PC4b**.

If all the pathways are compared, then the formation and decomposition of ROOOOR via two routes offers the most likely pathway to quinones with both having similar kinetic barriers. First, the single-step pathway (**I2** → **TS4c** → **P2c**) giving two quinones and hydrogen peroxide. Secondly, the two-step pathway (**I2** → **I4d** → **TS5d** → **P2a,b,d**), yielding a quinone, p-chinole and singlet oxygen. The single-step pathway is more favorable thermodynamically, with an exergonicity of the reaction of 28.12 kcal mol^{-1} lower. Nevertheless, both pathways have similar kinetic barriers. Thus, there is likely to be a distribution of products.

DLPNO-CCSD(T) calculations were performed for the pathways in this section, where the same reactive trend was observed, which validates our method chosen. The results are shown in Section 3 of the supporting information.

In real fuels, unsubstituted phenols form a majority of phenolic species. Nevertheless, they also form quinones when oxidized, and are expected to undergo similar reactions here.[38, 51] Nonetheless, this should be investigated further.

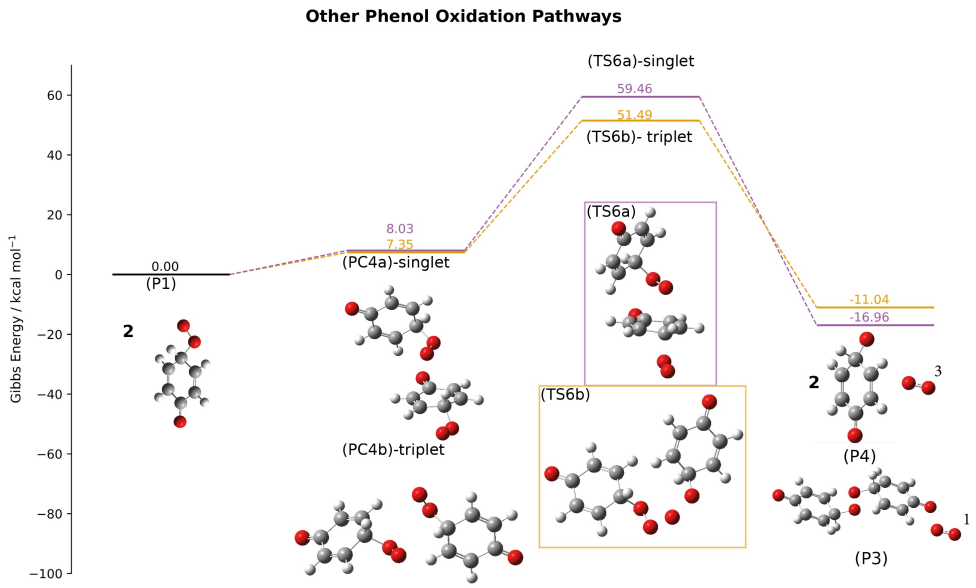

Figure 4: Reactions of Keto-Peroxyl Radical yielding non-quinone products on the triplet and singlet surfaces, calculated at the B3LYP-D3/cc-pVTZ *n*-Dodecane PCM level of theory

3.3. Quinone Heteroatom Coupling Step

3.3.1. Proposed SMORS Electrophilic Aromatic Substitution Step

The next step in the originally proposed SMORS mechanism; the electrophilic aromatic substitution (EAS) between indigenous electron-rich compounds and electrophilic quinones was found to be thermodynamically and kinetically prohibited. EAS reactions usually proceed with the initial attack of an electron-rich aromatic (the carbazole in this case) to an electron deficient species (quinone in our study), breaking aromaticity. The second step is the subsequent release of a species, most commonly H^+, at the site of electrophilic attack, completing the substitution reaction and re-establishing aromaticity.[52] The EAS between indole and benzoquinone (**P2**) proposed

by Beaver *et al.* is presented in Figure 5.[9]. Following the addition of benzoquinone, a zwitterionic σ-complex forms (Indole+Quinone-).[53]

Following the EAS scheme in Figure 5, no stable intermediate was found. The aprotic nature of n-dodecane solvent is unable to provide stability to the charged intermediate. However, even with a PCM water solvent model no stable benzoquinone-indole intermediate structure was found.

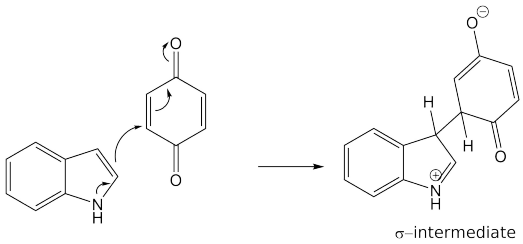

Figure 5: Proposed SMORS EAS step

Despite these limitations, the EAS transition state was identified between methyl substituted-carbazole proposed in Beaver *et al.*[9] and quinone, using a lower level of theory (B3LYP//cc-pvDZ). The intermediate product (**I4**) could only be obtained from a constrained optimization by freezing the C−C bonds. Without freezing the C−C bonds, the zwitterionic structure in 5 optimized to two separate indole and quinone species. The $\Delta_{\ddagger}G$=+177.11 kcal mol^{-1} barrier between benzoquinone and carbazole implies the original SMORS EAS proposal is kinetically prohibited. Recent work on EAS reactions indicate that in aprotic/apolar solvents interactions are likely to proceed through a concerted route, precluding the formation of a charged intermediate. The concerted routes studied found that in apolar solvents tend to involve autocatalysis of the attacking electrophile with another electrophile.[54, 55] Two quinone species reacting with a single indole was studied to explore an autocatalytic concerted route. However, in our case no concerted route to the coupled SMORS species was identified.

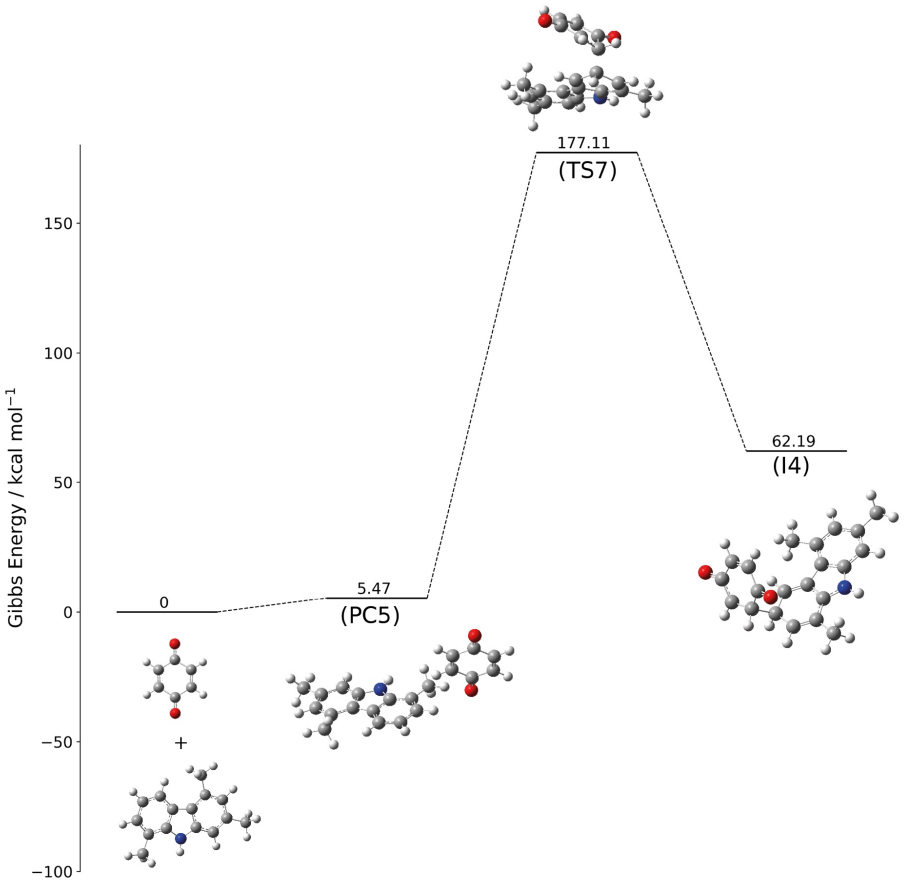

Figure 6: Potential energy surface (Gibbs free energy) of the reaction between carbazole and quinone, calculated at the B3LYP//cc-pVDZ *n*-Dodecane PCM level of theory.

3.3.2. Alternative Acid-Catalyzed EAS Step

The condensation reaction between benzoquinones and indoles has been reported previously to be catalyzed by acid.[56, 57] In fuels, it is proposed that the autoxidation of indigenous sulfur compounds can lead to the formation of sulfonic acids.[18] In addition, previous work has suggested that strong acids may play a role in catalyzing deposit formation.[2] Therefore, an acid-catalyzed pathway was considered as a possible route for SMORS formation.

This alternative SMORS scheme is presented in Figure 7. A protonated quinone was selected to model this pathway since protonation of the indole would preclude it from reacting with the electrophilic quinone species. From the overall reaction scheme presented in Figure 7, it can be concluded that a protonated quinone is able to proceed through a more favorable kinetic pathway. In addition, the formation of the aromatized hydroquinone carbazole species as proposed in the SMORS mechanism is possible and thermodynamically favorable ($-78.13\,\mathrm{kcal\,mol^{-1}}$).

The pre-reaction complex (**PC5**) for this reaction is exergonic. The barrier of the addition step (**TS7**) is small at $\Delta_{\ddagger}G$=+6.83 kcal mol^{-1} above **I5**. When compared to the non-catalyzed EAS scheme (Figure 5), the positive charge delocalized around the quinone species will activate the nucleophilic 3-position of the quinone. A hydrogen transfer (**TS8**) is then achieved through a pseudo-ring like structure, with a small barrier of $+7.10\,\mathrm{kcal\,mol^{-1}}$. The resultant structure from this hydrogen transfer contains a hydroquinone moiety (**I6**). The formation of this species is thermodynamically favorable with an Gibbs free energy change of -18.43 kcal mol^{-1} compared to the starting structures.

Protonation of quinone will also proceed with a barrier. In our DFT calculations the quinone was protonated by a dodecane sulfonic acid, known to form from the oxidation of indigenous sulfur compounds in fuel. It was found that the protonation step was barrierless but highly endergonic in n-dodecane with a large thermodynamic barrier of $\Delta_r G$=+77.57 kcal mol^{-1}. As shown in Figure 7, an overall Gibbs energy of -0.59 kcal mol^{-1} change is associated with the entire catalytic cycle, from the protonation of the quinone by the dodecane sulfonic acid to the formation of the SMORS species. This

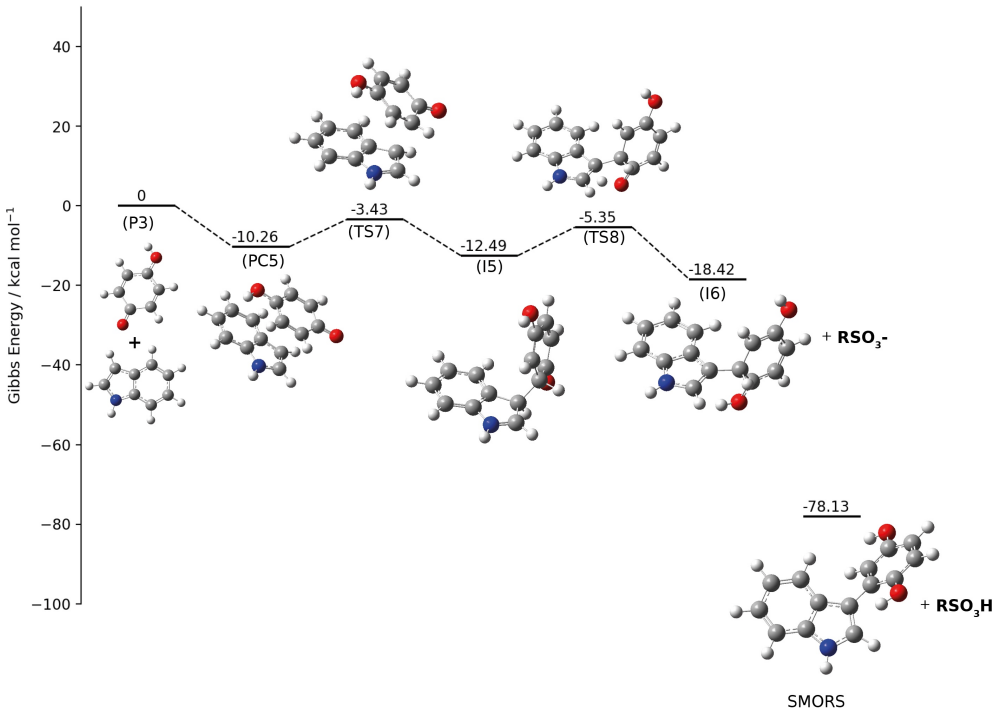

Figure 7: Acid catalyzed EAS step calculated at the B3LYP//cc-pVTZ n-Dodecane PCM level of theory.

indicates that the overall pathway is only mildly exergonic. Nevertheless, a protonated quinone allows the EAS step to proceed with modest kinetic barriers. However, with such a large thermodynamic barrier to quinone protonation in n-dodecane, protonation is unlikely unless the resultant ionic species are stabilized by a more polar solvent. The protonation step in water was calculated to have a thermodynamic cost of $\Delta_r G$=+25.43 kcal mol^{-1}. Small amounts of water have been detected as micelles in jet fuel.[58] We hypothesize that these micelles could offer a site for protonation in fuels.

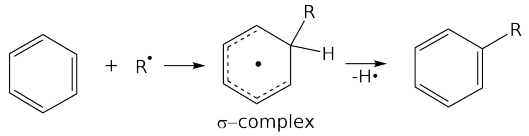

Figure 8: Generalized HAS mechanism.[61]

3.3.3. Alternative Oxidative Coupling Pathway

Although an acid catalyzed pathway was shown to proceed with modest kinetic barries, protonation of quinone in *n*-dodecane comes at a high thermodynamic cost. Therefore, we investigated additional mechanisms. Another possible pathway for the coupling between indoles and quinones in the SMORS mechanism is an oxidative coupling route. Oxidative coupling products have previously been detected in real and surrogate fuels.[38, 12] Undeniably, chain termination between an indole and a quinone radical would occur spontaneously. However, the termination of two dissimilar radical species is unlikely due to the low concentration of free-radicals in solution.[41, 59] Nevertheless, the termination reaction between an indole and a quinone radical will lead to a small proportion of SMORS. Alternatively, we investigated the possibility of a homolytic aromatic substitution (HAS) reaction between indole radicals and quinone, and indoles and quinone radicals. HAS has been described as the 'radical analogue of the more facile EAS'.[60] In our study an EAS pathway could not be located. Therefore HAS serves as another alternative pathway to forming the SMORS product.

The general HAS mechanism is presented in Figure 8. The first step is manifested by the attack of a radical species on an aromatic ring. The formation of a σ-complex (analogues to the Wheland intermediate in Figure 5) is then followed by the loss of hydrogen leading re-aromatization of the ring.

Following the HAS framework, the scheme depicted in Figure 8 is proposed for the reaction of quinone radical with an indole. The σ-complex formed from the initial attack of the quinone radical at the indole **C3** site is presented as **I8b**. It appears that the formation of the hydroquinone moiety is not immediately accessible *via* abstraction of a hydrogen atom from the σ-complex, which is how the general HAS mechanism proceeds (Figure 8). Instead, internal hydrogen transfer leads to the formation of intermediate **I9**, which contains a

semiquinone moiety. Semiquinones are known for their exceptional stability owing to their resonance stabilization.[37] Nevertheless, hydrogen abstraction from indigenous fuel compounds (RH in Figure 8) will lead to the formation of the SMORS product.

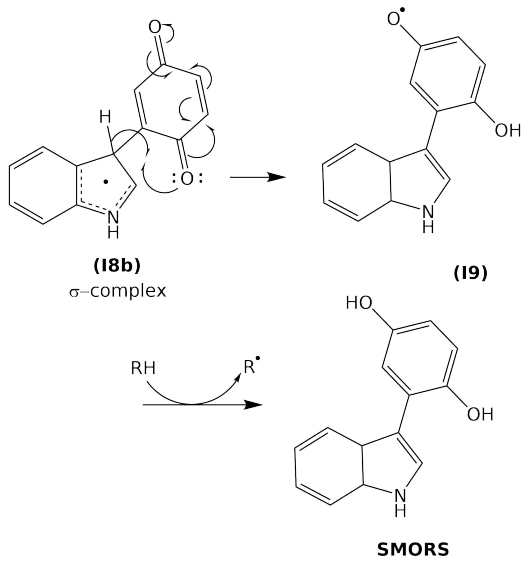

Figure 9: HAS mechanism applied to the SMORS indole + quinone substitution step

DFT calculations for the HAS pathway are presented in Figure 10. For comparison, two HAS reaction pathways were calculated for quinone and indole radicals respectively. For indole, multiple positions for hydrogen abstraction are available, but the **C3** is generally the preferred site for C-C bond formation.[62] Our calculations indicate that the route leading to the formation of quinone radicals is kinetically and thermodynamically preferred (**0→PC6b→TS9b→I7b**) over the formation indole radicals (**0→PC6a→TS9a→I7a**). The transition state for both species is characterized by a linear hydrogen transfer to a dodecane hydroxy radical, where the barrier to quinone hydrogen abstraction (**TS9b**) is 5.04 kcal mol^{-1} lower in Gibbs free energy than the indole abstraction barrier (**TS9a**). Additionally, the resultant quinone radical (**I7b**) is 8.12 kcal mol^{-1} lower in energy than the indole radical (**I7a**). Here it must be noted that when comparing all the products formed from the quinone production (**P2**), hydrogen abstraction

from p-chinole (**(a)P2**) is strongly preferred over quinone due to the formation of a highly stable semiquinone radical. Not shown in Figure 10, the abstraction of an α-hydrogen from p-chinole (**(a)P2**) has a $\Delta_{\ddagger}G$+5.54 kcal mol^{-1} barrier and a resultant $\Delta_r G$ −47.13 kcal mol^{-1}. Consequently, the p-chinole species is more likely to form radicals than indole and quinone here. However, the subsequent attack of the p-Chinole radical at the **C3** of an indole to form a HAS σ-complex has a high barrier $\Delta_{\ddagger}G$ 36.47 kcal mol^{-1}, meaning it can be precluded as a contributor to the HAS pathway.

The next step in the HAS scheme is the attack of the radical to the aromatic ring forming a σ-complex. With respect to the indole radical + quinone pathway, 1,4-benzoquinones are not strictly aromatic. Nevertheless, it has been noted that both substituted and non-substituted 1,4-benzoquinones are able to form resonance structures which could stabilize the resultant σ-intermediate.[63] Both the quinone and indole radical attack pathways (**I7**→**PC7**→**TS10**→**I8**) proceed exergonically. However, in relation to **I7**, the attack of a quinone radical has a lower free-energy barrier (**TS10b**) $\Delta_{\ddagger}G$=6.87 kcal mol^{-1} compared to the attack of the indole radical (**TS10a**) $\Delta_{\ddagger}G$=8.09 kcal mol^{-1}. For both **TS10a** and **TS10b**, the transition state is characterized by a rocking motion between the C−C bonds formed. The resultant indole radical-quinone σ-intermediate (**I8a**) is 4.84 kcal mol^{-1} more stable than the quinone radical-indole σ-intermediate (**I8b**).

Following the formation of the σ-intermediates, a subsequent hydrogen transfer leads both intermediates to form **I9** which is a stable semiquinone radical. Formation of **I9** is strongly preferred from quinone radical-indole σ-intermediate (**I8b**→**TS11b**→**I9**). The free energy barrier for **TS11b** is small ($\Delta_{\ddagger}G$=2.76 kcal mol^{-1}). The re-aromatization step **TS11b** for this pathway is characterized by a pseudo-cyclic transition state structure, where a hydrogen from the **C3** position on the indole is transferred to a quinone (=O) moiety ortho- to the C−C bond. By contrast, re-aromatization of the indole radical-quinone intermediate **I8b** proceeds via a high energy barrier (**TS11a**) $\Delta_{\ddagger}G$=47.64 kcal mol^{-1} meaning this pathway should be discounted as a major HAS pathway. **TS11a** is part of a hydrogen transfer from the quinone **C2** carbon, where the planar quinone moiety has to be bent to allow hydrogen transfer. This bending of the quinone moiety out-of-plane likely leads to the high barrier for **TS11a**.

The final step to produce the resultant **SMORS** species leading to re-

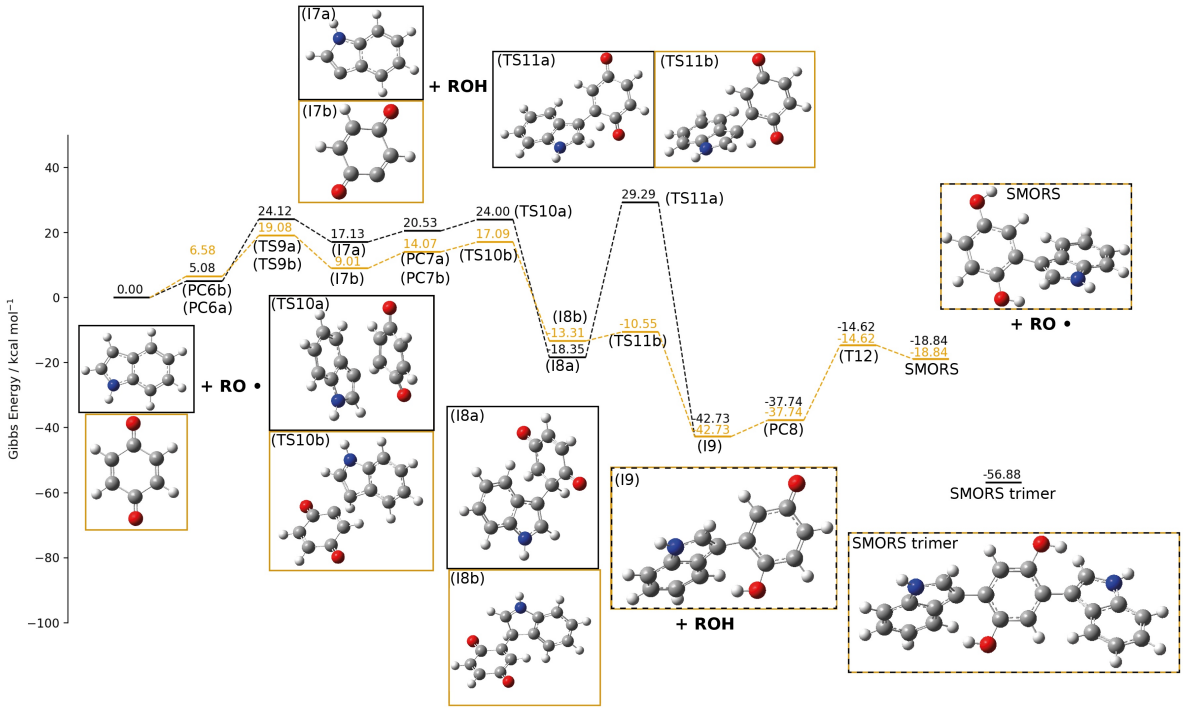

Figure 10: HAS step calculated at the B3LYP//cc-pVTZ n-dodecane PCM level of theory. The R group in this figure refers to an n-Dodecane moiety.

aromatization of the semiquinone compound **I9** via abstraction of hydrogen. Dodecanol produced in the first abstraction step (**0**→**TS9b**→**I7b**) was modelled as the species for hydrogen abstraction, allowing the efficiency of this radical propagation step to be assessed. The re-aromatization step with dodecanol proceeds endergonically (**I9**→**PC8**→**T12**→**SMORS**), showing the semiquinone compound **I9** is more stable than the dodecane hydroxy radical. However, overall the pathway to produce the final **SMORS** product is exergonic by -18.24 kcal mol^{-1} relative to the reactants state. This indicates this propagation cycle leading to SMORS is thermodynamically favorable. The stability of **I9** indicates that completion of the final re-aromatization step is disfavored. Formation of a SMORS trimer is likely given that the

SMORS trimer (Figure 12) is 14.15 kcal mol^{-1} more stable than **I9**. In this case an additional indole and dodecane hydroxy radical are consumed.

Our calculations show that SMORS can form under both acid catalyzed and oxidative conditions, in line with literature precedent.[64, 65] In order to investigate the formation of trimers under acid catalyzed and oxidative conditions a series of small scale testing was performed, as illustrated in the following section.

3.4. Flask Tests

Our calculations have shown that acid catalysis and/or oxidative conditions can lead to the formation of SMORS. To examine the effect of acids on the SMORS mechanism, two indole + phenol based model fuels were prepared, one containing acid forming dodecanethiol (IP-S) and one without (IP). The details of these tests are presented in the Supporting Information, in Section 4, along with a list of the molecular formula from (-)LCMS (negative mode LCMS), as well as the proposed structures. Each (-)LCMS peak was characterized in terms of species class by assigning the formula of the base peak to a species class. Subsequently, the areas associated with each class were grouped, allowing the % total area for each species class to be presented. This allows the relative abundance of each deposit class detected by (-)LCMS to be determined. The species classes and their associated percentage peak areas are presented in Figure 11a.

From (-)LCMS results, it is clear that the addition of thiol led to indole + sulfur oligomer formation, and suppressed the formation of SMORS. The heavy molecular weight materials corresponding to the IP-S surrogate contained compounds with molecular formulas associated with indole sulfonylation (**4**11b), arylated sulfonylation (**5**11b), and sulfenylation (**6**11b) reactions. These products have previously been detecting when indole and thiols have been combined under oxidative conditions.[62, 66, 54] A SMORS trimer (**1**11b) is directly observed in the IP surrogate deposit, suggesting that the SMORS process can proceed without the need of a strong acid catalyst, as weak carbxylic acids can still form from the autoxidation of bulk fuel.[67] This observation lends support to the HAS mechanism over an acid-catalyzed mechanism.

The formation of phenol dimers (**2**11b) in the sulfure-free IP surrogate deposit suggests that phenols are oxidized in the liquid phase. By contrast, no phenol oxidation products are observed in the sulfur containing IP-S surrogate. Instead, oxidized sulfur compounds form the largest proportion of the deposit. Co-elution of phenolic and oxidized sulfur compounds can be ruled out because phenolic compounds in IP elute at different retention times to oxidized sulfur compounds in IP-S (Tables 2 and 3 in the SI).

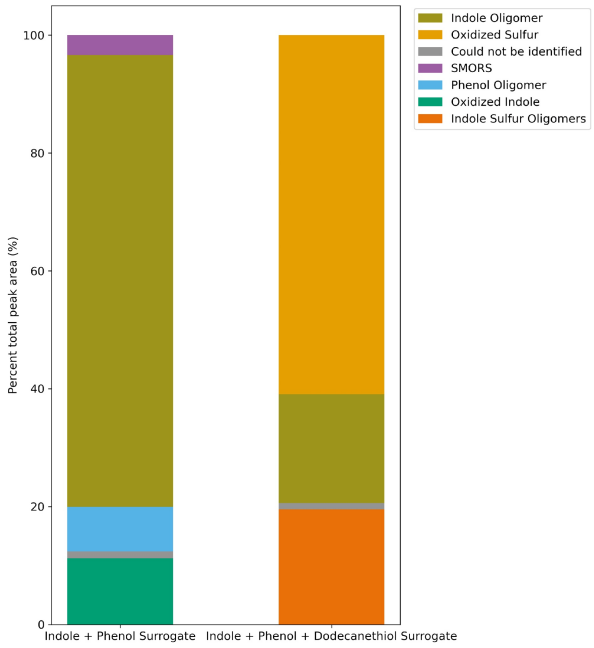

(a) (-)LCMS peak areas associated with the deposits generated from the n-dodecane $0.1\,\mathrm{mol\,L^{-1}}$ indole + phenol and $0.1\,\mathrm{mol\,L^{-1}}$ indole + phenol + dodecanethiol surrogates.

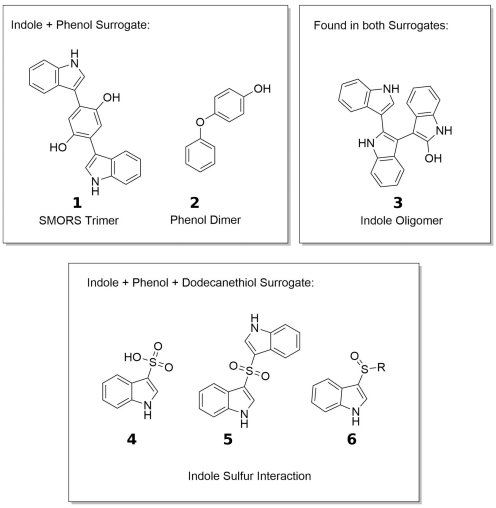

(b) Selected putative structures detected in the deposit. Detailed information of the deposit structures are present in Section 4 of the SI

Figure 11

3.5. Discussion and Implication for Fuels

The fact that different components in fuels interact with each other, either enhancing or slowing down deposit formation, is an uncontroversial idea. In fact, synergistic deposition enhancement between indole, phenol, and sulfur compounds in fuel has been observed in recent tests.[6] However, the mechanism by which this behind this synergistic behavior is still unclear. Our DFT and experimental results lead us to propose a modified SMORS mechanism. The first step in our mechanism is the oxidation of phenols (**1**) to quinones (**9**) are presented in Figure 3. The key weakness of the original SMORS proposal was the formation of quinones via a Russell Mechanism. Instead, we propose that quinones are produced via two main pathways, leading to a distribution of products. The first pathway, a two-step mechanism, involves the decomposition of the tetraperoxide (**5**) chain followed by hydrogen transfer. This leads to the production of one quinone (**7**), p-Chinole (**6**), and singlet oxygen (**8**). The second pathway, a single step-mechanism, involves the concerted decomposition of the tetraperoxide (**5**). This leads to the production of two quinones (**7**) and a hydrogen peroxide (**9**). The hydrogen peroxide (**9**) species is likely to undergo fission, yielding two HO$\cdot$ radicals, further propagating the chain-mechanism.

The second part of this modified SMORS mechanism is the coupling of quinone and indoles is proposed to occur via a HAS pathway, presented in Figure 13. The original EAS pathway, requires a stable, charged, σ-intermediate could not be located computationally in n-dodecane. Instead, a HAS pathway offers a route to a stable radical σ-intermediate via the attack of a quinone radical (**11**) on an indole (**13**). Quinone radicals could also attack other electron-rich fuel heterocyles like pyrroles and carbazoles, generalizing the scheme.

This is the first time a HAS pathway has been proposed as a route to fuel deposit formation. A HAS pathway also offers additional flexibility being a deposit formation which does not rely on free-radical termination to lead to C−C/C−O bond formation, and instead can be considered a propagation step. Beyond phenol and indole coupling, other fuel species could react to form via HAS reactions. A recent review focusing on HAS has shown these reactions can occur for both aromatic and heterocyclic compounds, including pyrrole and phenyls present in fuel. A particularly interesting facet of this review in relation to this work is the usage of SO_2 leaving groups for HAS coupling.[61] Indole containing SO_2/SO_3 leaving groups were directly observed

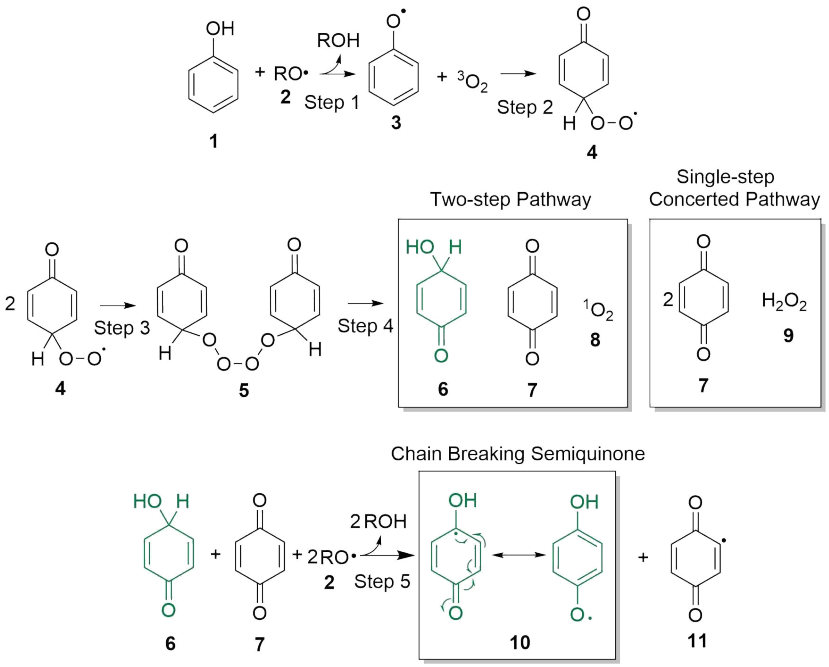

Figure 12: Modified SMORS mechanism: quinone production pathway

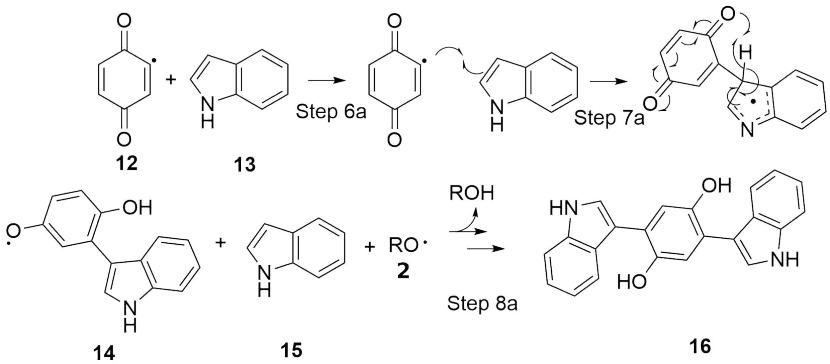

Figure 13: Modified SMORS mechanism: coupling mechanisms between indole and quinone

in the surrogate experiments (**4**,**5**11b).

The updated SMORS mechanism elucidated in this work will enable predictive aviation fuel stability mechanisms with higher accuracy. At present, existing predictive mechanisms contain no steps for nitrogen and phenol

interactions.[68, 1] This is largely due to the poor mechanistic understanding of the interactions between the species, despite the fact that deposition in conventional aviation fuels are highly correlated with nitrogen and phenol content.[7, 14] Additionally, a common weakness in existing pseudo-detailed mechanisms is implicit deposition steps. The work here presents an explicit generalized scheme for nitrogen and phenol deposit formation. The effect on kinetic and thermochemical parameters on the variations between different nitrogen species and different phenol structures using this generalized scheme can be studied, allowing for the eventual addition of explicit deposition steps in pseudo-detailed mechanisms.

4. Conclusions and Next Steps

The highly cited SMORS mechanism to explain phenol and fuel heteratom coupling in fuels was investigated by experimental and DFT methods. Several key modifications are made to the original proposed mechanism. First, in contrast to the proposed one-step Russell Mechanism, formation of quinone was shown to occur via a two-step mechanism. This occurs via the decomposition of a tetraperoxide, formed via the termination of two keto-peroxyl radicals, leading to two reactive hydroxy radicals and singlet oxygen. Hydroxy radicals then undergo a hydrogen transfer reaction to form quinone and a p-chinole, in contrast to the quinone, hydroquinone and triplet oxygen products in the original mechanism. The second important modification is the coupling step between quinone and electron-rich compounds. In apolar solvents, an electrophilic aromatic substitution (EAS) step was found to form unstable intermediates and was found to proceed with prohibitively high barriers. Instead, a homolytic aromatic substitution (HAS) mechanism was found to be the most likely pathway according to DFT calculated energies and experimental observations. Based on these findings, we propose a new modified SMORS pathway (Figures 12 and 13). Additionally, HAS reactions should begin to be explored as a new coupling pathway for fuel species.

5. Acknowledgements

References

[1] N. J. Kuprowicz, S. Zabarnick, Z. J. West, J. S. Ervin, Use of measured species class concentrations with chemical kinetic modeling for the

prediction of autoxidation and deposition of jet fuels, Energy and Fuels 21 (2) (2007) 530–544. doi:10.1021/ef060391o.

[2] R. N. Hazlett, J. A. Schreifels, W. M. Stalick, R. E. Morris, G. W. Mushrush, Distillate fuel insolubles: formation conditions and characterization, Energy and Fuels 5 (2) (1991) 269–273. doi:10.1021/ef00026a008.

[3] N. J. Kuprowicz, J. S. Ervin, S. Zabarnick, Modeling the liquid-phase oxidation of hydrocarbons over a range of temperatures and dissolved oxygen concentrations with pseudo-detailed chemical kinetics, Fuel 83 (13) (2004) 1795–1801. doi:10.1016/j.fuel.2004.03.013.
URL www.fuelfirst.com

[4] T. Jia, L. Pan, S. Gong, J. Xie, X. Wang, Y. Fang, J. J. Zou, X. Zhang, Mechanistic insights into the thermal deposition of highly thermal-stable jet fuel, Fuel 276 (May) (2020) 118100. doi:10.1016/j.fuel.2020.118100.
URL https://doi.org/10.1016/j.fuel.2020.118100

[5] J. W. Frankenfeld, W. F. Taylor, D. W. Brinkman, Storage stability of synfuels from oil shale. 1. general features of sediment formation in model fuel systems, Industrial and Engineering Chemistry Product Research and Development 22 (4) (1983) 608–614. doi:10.1021/i300012a018.

[6] S. Zabarnick, Z. J. West, L. M. Shafer, S. S. Mueller, R. C. Striebich, P. J. Wrzesinski, Studies of the role of heteroatomic species in jet fuel thermal stability: model fuel mixtures and real fuels, Energy and Fuels 33 (9) (2019) 8557–8565. doi:10.1021/acs.energyfuels.9b02345.

[7] L. M. Balster, S. Zabarnick, R. C. Striebich, L. M. Shafer, Z. J. West, Analysis of polar species in jet fuel and determination of their role in autoxidative deposit formation, Energy and Fuels 20 (6) (2006) 2564–2571. doi:10.1021/ef060275l.
URL https://pubs.acs.org/doi/abs/10.1021/ef060275l

[8] R. H. Clark, L. Smith, Further studies of the effects of polar compounds on the thermal stability of jet fuel, in: 3rd International Conference on Stability And Handling of Liquid Fuels, no. 2, 1988.

[9] B. Beaver, L. Gao, C. Burgess-Clifford, M. Sobkowiak, On the mechanisms of formation of thermal oxidative deposits in jet fuels. Are unified mechanisms possible for both storage and thermal oxidative deposit formation for middle distillate fuels?, Energy and Fuels 19 (4) (2005) 1574–1579. doi:10.1021/ef040090j.

[10] C. G. Kabana, S. Botha, C. Schmucker, C. Woolard, B. Beaver, Oxidative stability of middle distillate fuels. Part 1: Exploring the soluble macromolecular oxidatively reactive species (SMORS) mechanism with jet fuels, Energy and Fuels 25 (11) (2011) 5145–5157. doi:10.1021/ef200964z.

[11] M. Commodo, I. Fabris, C. P. T. Groth, Ö. L. Gülder, Analysis of aviation fuel thermal oxidative stability by electrospray ionization mass spectrometry (ESI-MS), Energy and Fuels 25 (5) (2011) 2142–2150. doi:10.1021/ef2002102.
URL https://pubs.acs.org/sharingguidelines

[12] R. Epping, S. Kerkering, J. T. Andersson, Influence of different compound classes on the formation of sediments in fossil fuels during aging, Energy and Fuels 28 (9) (2014) 5649–5656. doi:10.1021/ef501230c.

[13] K. M. Christison, R. M. Lorenz, L. Xue, O. D. Sparkman, Exploring the Molecular Origin of Jet Fuel Thermal Oxidative Instability through Statistical Analysis of Mass Spectral Data, Energy and Fuels 33 (2) (2019) 830–836. doi:10.1021/acs.energyfuels.8b03670.
URL https://pubs.acs.org/sharingguidelines

[14] M. Sobkowiak, J. M. Griffith, B. Wang, B. Beaver, Insight into the mechanisms of middle distillate fuel oxidative degradation. Part 1: On the role of phenol, indole, and carbazole derivatives in the thermal oxidative stability of fischer-tropsch/petroleum jet fuel blends, Energy and Fuels 23 (4) (2009) 2041–2046. doi:10.1021/ef8006992.
URL http://pubs.acs.org/doi/abs/10.1021/ef8006992

[15] D. R. Hardy, M. A. Wechter, Insoluble sediment formation in middle distillate diesel fuel: further evidence concerning the role of in situ fuel acidity, Fuel 69 (6) (1990) 720–724. doi:10.1016/0016-2361(90)90036-P.

[16] C. M. Parks, E. Alborzi, S. G. Blakey, A. J. Meijer, M. Pourkashanian, Density Functional Theory Calculations on Copper-Mediated Peroxide Decomposition Reactions: Implications for Jet Fuel Autoxidation, Energy and Fuels 34 (6) (2020) 7439–7447. doi:10.1021/acs.energyfuels.0c00918.

[17] S. Zabarnick, D. K. Phelps, Density functional theory calculations of the energetics and kinetics of jet fuel autoxidation reactions, Energy and Fuels 20 (2) (2006) 488–497. doi:10.1021/ef050348l.
URL https://pubs.acs.org/doi/full/10.1021/ef050348l?src=recsys

[18] C. M. Parks, A. J. Meijer, S. G. Blakey, E. Alborzi, M. Pourkashanian, Computational studies on the reactions of thiols, sulfides and disulfides with hydroperoxides. Relevance for jet fuel autoxidation, Fuel 316 (January) (2022) 123326. doi:10.1016/j.fuel.2022.123326.
URL https://doi.org/10.1016/j.fuel.2022.123326

[19] E. Alborzi, M. R. Dwyer, C. M. , A. Sheikhansari, D. C. Mielczarek, M. Zanganeh, A. J. Meijer, S. G. Blakey, M. Pourkashanian, Construction of a reduced chemical kinetic mechanism for autoxidation of n-paraffinic solvent – A model for aviation fuel, Fuel 294 (January) (2021) 120170. doi:10.1016/j.fuel.2021.120170.
URL https://doi.org/10.1016/j.fuel.2021.120170

[20] P. Hohenberg, W. Kohn, Inhomogenous Electron Gas, Physical Review 136 (1964) 864–871. doi:10.1007/BF01198136.
URL https://journals.aps.org/pr/pdf/10.1103/PhysRev.136.B864

[21] M. J. Frisch, G. W. Trucks, H. B. Schlegel, G. E. Scuseria, M. A. Robb, J. R. Cheeseman, G. Scalmani, V. Barone, B. Mennucci, G. A. Petersson, H. Nakatsuji, M. Caricato, X. Li, H. P. Hratchian, A. F. Izmaylov, J. Bloino, G. Zheng, J. L. Sonnenberg, M. Hada, M. Ehara, K. Toyota, R. Fukuda, J. Hasegawa, M. Ishida, T. Nakajima, Y. Honda, O. Kitao, H. Nakai, T. Vreven, J. A. Montgomery, Jr., J. E. Peralta, F. Ogliaro, M. Bearpark, J. J. Heyd, E. Brothers, K. N. Kudin, V. N. Staroverov, R. Kobayashi, J. Normand, K. Raghavachari, A. Rendell, J. C. Burant, S. S. Iyengar, J. Tomasi, M. Cossi, N. Rega, J. M. Millam, M. Klene, J. E.

Knox, J. B. Cross, V. Bakken, C. Adamo, J. Jaramillo, R. Gomperts, R. E. Stratmann, O. Yazyev, A. J. Austin, R. Cammi, C. Pomelli, J. W. Ochterski, R. L. Martin, K. Morokuma, V. G. Zakrzewski, G. A. Voth, P. Salvador, J. J. Dannenberg, S. Dapprich, A. D. Daniels, Ö. Farkas, J. B. Foresman, J. V. Ortiz, J. Cioslowski, D. J. Fox, Gaussian 09 Revision E.01, gaussian Inc. Wallingford CT 2009 (2009).

[22] A. D. Becke, Density-functional thermochemistry. III. The role of exact exchange, The Journal of Chemical Physics 98 (7) (1993) 5648–5652. doi:10.1063/1.464913.

[23] S. Grimme, S. Ehrlich, L. Goerigk, Effect of the damping function in dispersion corrected density functional theory, Journal of computational chemistry 32 (7) (2011) 1456–1465.

[24] S. Miertuš, E. Scrocco, J. Tomasi, Electrostatic interaction of a solute with a continuum. a direct utilizaion of ab initio molecular potentials for the prevision of solvent effects, Chemical Physics 55 (1) (1981) 117–129.

[25] T. H. Dunning Jr, Gaussian basis sets for use in correlated molecular calculations. i. the atoms boron through neon and hydrogen, The Journal of chemical physics 90 (2) (1989) 1007–1023.

[26] S. Grimme, Supramolecular binding thermodynamics by dispersion-corrected density functional theory, Chemistry–A European Journal 18 (32) (2012) 9955–9964.

[27] R. F. Ribeiro, A. V. Marenich, C. J. Cramer, D. G. Truhlar, Use of solution-phase vibrational frequencies in continuum models for the free energy of solvation, The Journal of Physical Chemistry B 115 (49) (2011) 14556–14562.

[28] R. Paton, Goodvibes (2016).
URL https://github.com/patonlab/GoodVibes

[29] C. Riplinger, F. Neese, An efficient and near linear scaling pair natural orbital based local coupled cluster method, The Journal of chemical physics 138 (3) (2013) 034106.

[30] C. Riplinger, B. Sandhoefer, A. Hansen, F. Neese, Natural triple excitations in local coupled cluster calculations with pair natural orbitals, The Journal of chemical physics 139 (13) (2013) 134101.

[31] C. Riplinger, P. Pinski, U. Becker, E. F. Valeev, F. Neese, Sparse maps—a systematic infrastructure for reduced-scaling electronic structure methods. ii. linear scaling domain based pair natural orbital coupled cluster theory, The Journal of chemical physics 144 (2) (2016) 024109.

[32] M. Saitow, U. Becker, C. Riplinger, E. F. Valeev, F. Neese, A new near-linear scaling, efficient and accurate, open-shell domain-based local pair natural orbital coupled cluster singles and doubles theory, The Journal of chemical physics 146 (16) (2017) 164105.

[33] Y. Guo, C. Riplinger, U. Becker, D. G. Liakos, Y. Minenkov, L. Cavallo, F. Neese, Communication: An improved linear scaling perturbative triples correction for the domain based local pair-natural orbital based singles and doubles coupled cluster method [dlpno-ccsd (t)], The Journal of chemical physics 148 (1) (2018) 011101.

[34] F. Neese, F. Wennmohs, U. Becker, C. Riplinger, The ORCA quantum chemistry program package, Journal of Chemical Physics 152 (22) (2020). doi:10.1063/5.0004608.
URL https://doi.org/10.1063/5.0004608

[35] M. Dwyer, S. Blakey, E. Alborzi, A. Meijer, The role of hydrocarbon composition on the thermal stability of aviation fuels, in: IASH 2017, the 15th International Symposium on Stability, Handling and Use of Liquid Fuels Rome,, no. September, 2017. doi:10.1021/ja111674c.

[36] D. Min, J. Boff, Chemistry and reaction of singlet oxygen in foods, Comprehensive reviews in food science and food safety 1 (2) (2002) 58–72.

[37] B. Dellinger, S. Lomnicki, L. Khachatryan, Z. Maskos, R. W. Hall, J. Adounkpe, C. McFerrin, H. Truong, Formation and stabilization of persistent free radicals, Proceedings of the Combustion Institute 31 I (1) (2007) 521–528. doi:10.1016/j.proci.2006.07.172.

[38] L. Jones, N. C. Li, Ageing of SRC II middle distillate from Illinois No. 6 coal, Fuel 62 (10) (1983) 1156–1160. doi:10.1016/0016-2361(83)90057-1.

[39] H. Shadnia, J. S. Wright, Understanding the toxicity of phenols: Using quantitative structure-activity relationship and enthalpy changes to discriminate between possible mechanisms, Chemical Research in Toxicology 21 (6) (2008) 1197–1204. doi:10.1021/tx800058r.

[40] M. Michalík, P. Poliak, V. Lukeš, E. Klein, From phenols to quinones: Thermodynamics of radical scavenging activity of para-substituted phenols, Phytochemistry 166 (July) (2019) 112077. doi:10.1016/j.phytochem.2019.112077.
URL https://doi.org/10.1016/j.phytochem.2019.112077

[41] E. T. Denisov, I. B. Afanas' ev, Oxidation and antioxidants in organic chemistry and biology, CRC press, 2005.

[42] G. A. Russell, Deuterium-isotope effects in the autoxidation of aralkyl hydrocarbons. mechanism of the interaction of peroxy radicals1, Journal of the American Chemical Society 79 (14) (1957) 3871–3877.

[43] R. Lee, G. Gryn'Ova, K. U. Ingold, M. L. Coote, Why are: Sec -alkylperoxyl bimolecular self-reactions orders of magnitude faster than the analogous reactions of tert -alkylperoxyls? the unanticipated role of CH hydrogen bond donation, Physical Chemistry Chemical Physics 18 (34) (2016) 23673–23679. doi:10.1039/c6cp04670c.

[44] K. Adamic, J. A. Howard, K. U. Ingold, Absolute rate constants for hydrocarbon autoxidation. XVI. Reactions of peroxy radicals at low temperatures, Canadian Journal of Chemistry 47 (20) (1969) 3803–3808. doi:10.1139/v69-634.
URL www.nrcresearchpress.com

[45] A. R. Smith, S. Di Muzio, F. Ramondo, G. Meloni, Peroxy self-reaction leading to the formation of furfural, Physical Chemistry Chemical Physics 21 (20) (2019) 10228–10237. doi:10.1039/c8cp07571a.

[46] J. Howard, J. Bennett, The self-reaction of sec-alkylperoxy radicals: a kinetic electron spin resonance study, Canadian Journal of Chemistry 50 (14) (1972) 2374–2377.

[47] G. Mendenhall, E. Quinga, Deuterium isotope cage effects in the dismutation of alkoxyl radicals. significance for the mode of alkylperoxyl termination, International journal of chemical kinetics 17 (11) (1985) 1187–1190.

[48] E. Quinga, G. Mendenhall, Chemiluminescence from hyponitrite esters. excited triplet states from dismutation of geminate alkoxyl radical pairs, Journal of the American Chemical Society 105 (21) (1983) 6520–6521.

[49] J. Helberg, D. A. Pratt, Autoxidation vs. antioxidants-the fight for forever, Chemical Society Reviews 50 (13) (2021) 7343–7358. doi:10.1039/d1cs00265a.

[50] M. Dwyer, Investigating The Role Of Aviation Fuels Hydrocarbon Chemistry On Its Autoxidation, Ph.D. thesis, University of Sheffield (2019).

[51] T. Jia, M. Zhao, L. Pan, C. Deng, J. J. Zou, X. Zhang, Effect of phenolic antioxidants on the thermal oxidation stability of high-energy–density fuel, Chemical Engineering Science 247 (2022) 117056. doi:10.1016/j.ces.2021.117056.
URL https://doi.org/10.1016/j.ces.2021.117056

[52] R. E. Gawley, A proposal for (slight) modification of the hughes-ingold mechanistic descriptors for substitution reactions, Tetrahedron letters 40 (23) (1999) 4297–4300.

[53] S. L. Matlow, G. W. Wheland, Orientation in Aromatic Substitution: A Theoretical Study of the Competition between Groups, Journal of the American Chemical Society 77 (13) (1955) 3653–3655. doi:10.1021/ja01618a073.

[54] Hongchang, Sulfonation mechanism of benzene with SO3 in sulfuric acid or oleum or aprotic solvent: Obeying the transition state theory via a trimolecular electrophilic substitution clarified by density functional theory calculation, Computational and Theoretical Chemistry 1112 (2017) 111–122. doi:10.1016/j.comptc.2017.04.012.
URL http://dx.doi.org/10.1016/j.comptc.2017.04.012

[55] T. Stuyver, D. Danovich, F. De Proft, S. Shaik, Electrophilic Aromatic Substitution Reactions: Mechanistic Landscape, Electrostatic and

Electric-Field Control of Reaction Rates, and Mechanistic Crossovers, Journal of the American Chemical Society 141 (24) (2019) 9719–9730. doi:10.1021/jacs.9b04982.

[56] M. C. Pirrung, L. Deng, Z. Li, K. Park, Synthesis of 2, 5-dihydroxy-3-(indol-3-yl) benzoquinones by acid-catalyzed condensation of indoles with 2, 5-dichlorobenzoquinone, The Journal of Organic Chemistry 67 (24) (2002) 8374–8388.

[57] M. G. Corradini, C. Costanini, G. Prota, T. Schultz, Acid-catalyzed reactions of indoles with 1, 4-quinones., ChemInform 20 (33) (1989).

[58] S. Baena-Zambrana, S. L. Repetto, C. P. Lawson, J. K. Lam, Behaviour of water in jet fuel - A literature review, Progress in Aerospace Sciences 60 (2013) 35–44. doi:10.1016/j.paerosci.2012.12.001.

[59] S. P. Heneghan, S. Zabarnick, Oxidation of jet fuels and the formation of deposit, Fuel 73 (1) (1994) 35–43. doi:10.1016/0016-2361(94)90185-6.
URL https://www.sciencedirect.com/science/article/pii/0016236194901856

[60] M. Gurry, F. Aldabbagh, A new era for homolytic aromatic substitution: Replacing Bu3SnH with efficient light-induced chain reactions, Organic and Biomolecular Chemistry 14 (16) (2016) 3849–3862. doi:10.1039/c6ob00370b.

[61] W. R. Bowman, J. M. Storey, Synthesis using aromatic homolytic substitution—recent advances, Chemical Society Reviews 36 (11) (2007) 1803–1822. doi:10.1039/b605183a.

[62] S. Liu, F. Zhao, X. Chen, G. J. Deng, H. Huang, Aerobic oxidative functionalization of indoles, Advanced Synthesis and Catalysis 362 (18) (2020) 3795–3823. doi:10.1002/adsc.202000285.

[63] M. Nonella, A Generalized Resonance Model for Substituted 1,4-Benzoquinones, Journal of Physical Chemistry A 103 (35) (1999) 7069–7075. doi:10.1021/jp9907847.

[64] J. S. Yadav, B. V. Reddy, T. Swamy, InBr3-Catalyzed Conjugate Addition of Indoles to p-Quinones: An Efficient Synthesis of 3-Indolylquinones, Synthesis 44 (1) (2004) 106–110. doi:10.1055/s-2003-44364.

[65] J. Stejskal, P. Bober, M. Trchová, J. Horský, Z. Walterová, S. K. Filippov, T. Plachý, M. Mrlík, Oxidation of pyrrole with: P -benzoquinone to semiconducting products and their application in electrorheology, New Journal of Chemistry 42 (12) (2018) 10167–10176. doi:10.1039/c8nj01283k.

[66] F. Takahashi, K. Nogi, H. Yorimitsu, Catalytic inter- and intramolecular coupling of aryl sulfones, Phosphorus, Sulfur and Silicon and the Related Elements 194 (7) (2019) 742–745. doi:10.1080/10426507.2019.1603232.
URL https://doi.org/10.1080/10426507.2019.1603232

[67] B. D. Boss, R. N. Hazlett, Oxidation of hydrocarbons in the liquid phase: n-dodecane in a borosilicate glass chamber at 200 °C, Canadian Journal of Chemistry 47 (1969) 4176–4182.

[68] Z. Liu, S. Tang, Z. Li, Z. Qin, S. Yuan, L. Wang, L. Wang, X. Zhang, G. Liu, An improved kinetic model for deposition by thermal oxidation of aviation hydrocarbon fuels, Fuel 258 (June) (2019) 116139. doi:10.1016/j.fuel.2019.116139.
URL https://doi.org/10.1016/j.fuel.2019.116139

Declaration of interests

☐The authors declare that they have no known competing financial interests or personal relationships that could have appeared to influence the work reported in this paper.

☒The authors declare the following financial interests/personal relationships which may be considered as potential competing interests:

Charlie Adams reports financial support was provided by The University of Sheffield Department of Mechanical Engineering.

Credit Author Statement

Author	Credit
Charlie Adams	Conceptualization, Methodology, Investigation, Writing - Original Draft, Visualization
Ehsan Alborzi	Writing - Review & Editing, Funding acquisition, Project Administration
Anthony J.H.M. Meijer	Writing - Review & Editing, Methodoloy
Kevin J. Hughes	Writing - Review & Editing
Mohamed Pourkashanian	Funding acquisition